

Quantum Control of Rydberg Atoms

Sondre Eliasson

Master Thesis in Nano Science



University of Bergen, Norway
Department of Physics and Technology
2014

Abstract

In 2007 the AEGIS experiment was started at CERN with the goal to determine the gravitational acceleration of the antihydrogen atom. This is achieved through accelerating the antihydrogen atoms toward a detector and measure the path of flight. To achieve the desired accuracy of the measurement, a large enough amount of antihydrogen atoms have to reach the detector. To obtain this objective, the use of quantum polarization control has been put forward. [1]

The main obstacle turns out to be the large unknown number of initial states, the limited numbers of coupling and the symmetry of the dynamics. In the thesis, quantum control in the time domain is described and applied to Rydberg atoms. A code has been modified and extended with respect to unknown initial conditions. Several applications of the code illustrate the given challenge. In addition, controlled excitation (or de-excitation) indicate that increased initial polarization can be achieved.

Forord

Denne oppgåva er det endelege resultatet av mastergraden etter to års forskning og studier ved gruppa for optikk og atomfysikk ved Universitetet i Bergen. Dessverre kan den ikkje formidle alt av opplevelsar, oppdagingar og grå hår som eg har støtt på i løpet av desse åra. Eg følar meg svært heldig for å fått tilbragt denne tida blant så mange hyggelege og flinke mennesker, og det er fleire som har ein liten del av æra for denne oppgåva.

Den største takken går sjølvstilt til min veileder Jan Petter Hansen. Takk for å ha vist meg det spennande feltet kvantekontroll og leda meg gjennom denne oppgåva. Eg har satt stor pris på ditt sosiale, så vel som faglege, engasjement. Eg vil også sende ein takk til min biveileder, Lene Sælen, som gjennom sitt tidlegare arbeid har bidratt til at denne oppgåva har vore mogleg.

I løpet av oppgåva har det vore store utskiftningar blant beboarane i 2.etasje (og ikkje minst med etasjen sjølv), og eg vil takke alle dei eg har fått moglegheit til å bli kjent med. Ein takk til Aleksander, Arne og resten av doktorgradstudentane for å tatt meg godt i mot og hjulpet meg med alt eg har spurt om. Takk også til Morten og Øyvind som har vist meg tillit og tildelt meg oppgåver utover studiene. Ein fast glede det siste året har vore lunsjprosjektet og eg vil takke alle de som har vore med på denne hyggelege samankomsten.

Ein takk til alle dei som eg i løpet av graden har delt kontoret med. Takk til Therese som overbeviste meg om å begynne med atomfysikk, og takk til Espen som tok over plassen etterpå. Ein spesiell takk går til Lars som har vore ledsager og sparringspartner gjennom heile løpet. Gjennom mastergraden har eg vore på nokon konferansar, og eg er svært takknemleg for å fått midlar frå NordForsk til dette.

Takk til familien min heime i Florø som heile tida vore interessert i korleis det går, og som har vore oppmuntrande sjølv i dei tyngste stunder. Til slutt ein stor takk til min kjæraste og med-masterstudent Inga som har vore den viktigaste støttespelaren gjennom denne viktige tida i våre liv. Inga, du er den verkelege MVP.

Sondre

Contents

1	Introduction	11
1.1	Background	11
1.2	Antimatter	12
1.3	The AEGIS experiment	13
1.4	Quantum control to control polarization	15
1.5	Outline and outlook	16
2	Theory	17
2.1	Optimal control theory	17
2.1.1	Theory	17
2.1.2	Classical example - the triangle problem	18
2.2	Quantum mechanics	19
2.2.1	One dimensional asymmetrical well	21
2.3	Electromagnetic fields	24
2.4	Quantum control	24
2.4.1	Algorithm scheme	27
2.4.2	Laser field constraints	28
3	One Dimensional Asymmetrical Well	31
3.1	Single transition	31
3.2	Multiple initial states	36
3.3	Summary	45
4	Two Dimensional Hydrogen Atom	47
4.1	Polar coordinates and separation of variables	47
4.2	Optimization example for $n=5$	51
4.3	Comparison of individual and joint optimization for initial state in $\Psi_{n=5,m=-4}$ and $\Psi_{n=5,m=4}$	58
4.4	Summary	62
5	Three Dimensional Hydrogen in Magnetic Field	63
5.1	The three-dimensional Coulomb problem	63
5.1.1	Angular Solutions	64
5.1.2	Radial solutions	65
5.2	Matrix elements for hydrogen in a magnetic field	67
5.3	Optimization of hydrogen atom polarization in magnetic field	68
5.4	Target level optimization	73

5.5 Summary	78
6 Conclusion and Outlook	79
Appendix	
A Atomic Units	81
B Simulation Matrices	83
B.1 Two dimensional hydrogen optimization	83
B.2 Three dimensional hydrogen optimization	84
B.2.1 3-level matrices	84
B.2.2 3- and 4-level matrices	85
C Programs	89
C.1 1D asymmetrical well	89
C.2 2D hydrogen atom	89
C.3 3D hydrogen atom in magnetic field	89
C.4 Visualisation program	90
C.5 Converter	90

List of Figures

1.1	AEGIS experimental setup	14
2.1	The triangle problem	19
2.2	The asymmetrical well	23
3.1	1D initial and target states	32
3.2	1D asymmetrical well distribution result	33
3.3	1D yield and functional development	35
3.4	1D initial and final field	36
3.5	1D two initial states, distribution result	38
3.6	1D two initial states, density development	39
3.7	1D two initial states, yield and functional development	40
3.8	1D two initial state optimal field	41
3.9	The optimized field for the 1D state 3 to state 2 optimization	42
3.10	The pulsetrain for the 1D states 1 and 3 to state 2 optimization	43
3.11	Population distribution in the 1D states after pulsetrain	44
4.1	Radial distribution for the 2D hydrogen n=5 states	52
4.2	The real part of the 2D hydrogen n=5 basis wavefunctions	53
4.3	The 2D hydrogen n=5 polarized states	54
4.4	The development of the yield and functional for the 2D n=5 optimization	56
4.5	The final states for the 2D hydrogen n=5 optimization	57
4.6	The final population distribution for the 2D n=5 optimization	58
4.7	The final population distribution for the two separated 2D n=5 optimizations	60
4.8	The final polarization for the two separated 2D n=5 optimizations	60
4.9	The final population distribution for the joint 2D n=5 optimization	61
4.10	The final polarization for the joint 2D n=5 optimization	61
5.1	The magnetic splitting of the energy for the n=3 atomic states	69
5.2	The initial test pulse used in the 3D optimizations	71
5.3	The yield and functional development for the n=3 atomic optimization	72
5.4	The final field found in the atomic n=3 optimization	73
5.5	The magnetic splitting of the energy for the atomic n=3 and 4 states	74
5.6	The development of the field and functional for the atomic multitarget optimization	76
5.7	The final field for the atomic multitarget optimization	77

Chapter 1

Introduction

1.1 Background

There is no better measurement of the progress in science than our conquest and control of the dimensions. Our ancestors could see the sun and some of the planets, and had myths about our creation. They even had an idea about an indivisible unit called an atom. However, there is no doubt that they would have been surprised to find that we now can study galaxies billions of lightyears away and even try to reconstruct the beginning of the universe. The most astonishing achievement is perhaps how small the things we can study are. We can explain what an atom consists of and study its properties. Today we are not content with only studying atoms, we also want to control and use them, one by one.

The idea of control at atomic scale was introduced by Richard Feynman¹ in 1959 when he held his famous speech "There is plenty of room at the bottom" [3]. There he foretold the possibility of creating materials and structures atom by atom and stated that this was an inevitable development of science. This was the start of the field that was to be known as nanotechnology². Nanotechnology is hard to define, but its broadest and most general definition is as found in the European Union code of conduct for responsible nanotechnology:

Nanotechnology and Nano science research encompasses all research activities dealing with matter at the nanometric scale (1 to 100 nm) [5].

To achieve control at this scale it is necessary with the right equipment, and instruments with better and better resolution have been developed [6]. In 1970 separate atoms were seen for the first time by Crewe et al. [7]. Later the scanning tunnelling microscope (STM) [8] and the atomic force microscope (AFM) were invented [9] making it possible to study surfaces with extremely high resolution. What more, they were soon showed to be able to manipulate atoms. In 1989 Don Eigler at the IBM used the STM to position

¹Richard Feynman(1918-1988) shared the Nobel prize in 1965 for "fundamental work in quantum electrodynamics" [2].

²Coined by Norio Taniguchi(1912-1999) in 1974 [4].

35 Xenon atoms to form the IBM logo [10]. STM has also been used to influence the electronic structure of atoms and promote bond-forming and -breaking by adding or remove electrons. The diversity in the applications of STM has made it an important tool within nanotechnology.

One of the most difficult aspects of control on the nanoscale is also one of the properties that makes nanotechnology so interesting. When the objects we are studying are at a very small scale, they cannot really be seen as clearly defined objects, but behave more like waves. This means that we cannot use classical mechanics to do calculations on them, instead we rely on quantum mechanics. This theory was introduced in the 20th century to try to describe some results that were unexplained by classical mechanics. In 1926, Erwin Schrödinger published his paper on "An Undulatory Theory of the Mechanics of Atoms and Molecules" [11]. In this article he formulated what has later been known as the time dependent Schrödinger equation (TDSE). The solution of the Schrödinger equation is a wave function that is the most general description of the quantum mechanical system. Together with Einstein's and Planck's³ theories about quantized energy packets [14] [15] and Heisenberg's uncertainty principle [16] this laid the ground work for quantum mechanics as a theory to explain the behaviour of particles at atomic and subatomic scale. As a mathematical description for the atomic world, this theory introduced us to new physical phenomena like wave-particle duality, quantum entanglement and later, antimatter.

1.2 Antimatter

In 1928, Paul Dirac⁴ presented his paper "The quantum theory of the electron" where the Dirac equation was first published [20]. The equation combines both the quantum theory and special relativity, allowing the behaviour of electrons moving at relativistic speed to be calculated. The equation also has two solutions, one for electrons with positive energy and one for electrons with negative energy. This predicted the existence of antiparticles for the first time. Antiparticles are the building blocks of antimatter in the same way that matter consists of particles. Antiparticles have the same mass and the same magnitude of charge and spin as their corresponding particles. However, they have opposite sign for the charge as well as other particle properties. When antimatter and matter collides they can annihilate and release energy corresponding to their mass as explained by Einstein's law of energy-mass equivalence, $E = mc^2$.

In 1932, Carl Anderson discovered the positron, the antiparticle of the electron, proving the prediction of Dirac [21]. Following this, research has sequentially discovered the different antiparticles the antiatom consists of [22] [23] [24]. In 1995 the first antihydrogen was produced in the "Low Energy Antiproton Ring" at CERN [25] and in 2011 it was confirmed that CERN had been able to trap antihydrogen for 1000 seconds [26]. This

³Albert Einstein(1879-1955), Nobel prize in 1965 "for his services to Theoretical Physics" [12], and Max Planck(1858-1957) , Nobel prize in 1921 for "his discovery of energy quanta" [13].

⁴Paul Dirac(1902-1984) and Erwin Schrödinger(1887-1961) won the Nobel prize in 1933 "for the discovery of new productive forms of atomic theory" [17] [18], while Werner Heisenberg(1901-1976) at the same time was awarded the 1932 Nobel prize "for the creation of quantum mechanics" [19].

allowed for the first time detailed studies of antimatter and comparisons with normal matter.

Antihydrogen is the simplest antiatom and the antiparticle of hydrogen. The hydrogen atom is one of the best understood physical systems as well as the most abundant element. It has only one electron and one electron-nucleus interaction and the Schrödinger equation can be exactly solved for the system. The equation can successfully reproduce the spectral line of the hydrogen atom, responding to the energy levels in the Bohr model. Since we have such a throughout insight to the hydrogen atom, we have many properties we can compare to the antihydrogen and from them we can search for differences between matter and antimatter.

One of the differences regarding matter and antimatter is that there seems to be only matter left. When the universe was created it is believed that both matter and antimatter were created, but now it seems like matter greatly outnumber antimatter. The general perception is that there was an asymmetry when the universe was created and what we can see around us is the surplus of matter that was created. This asymmetry in the universe is called the *Baryon asymmetry problem* [27] and there is not yet any scientific proved explanation for why there should be an asymmetry. The lack of complete answers has led to different theories to explain the abundance of matter. One theory is the existence of antigravity. In the same way as matter attracts itself, the theory says that antimatter should attract antimatter. However the idea is that there also will be a repulsion or an altered attraction between antimatter and normal matter [28] [29]. If this theory is correct it could explain why we can only find normal matter. There exists an equal amount of matter and antimatter, but they repel each other and has therefore not been able to react. There can exist galaxies containing only antimatter, but from far away we are not able to distinguish them from normal matter because they emit identical photons. While the general consensus is that there is no difference in gravity between matter and antimatter, it is a question that begs to be answered. To try to answer the question experimentally, the Antimatter Experiment: Gravity, Interferometry, Spectroscopy (AEGIS) project was established at CERN in 2007.

1.3 The AEGIS experiment

The AEGIS experiment [1] is a modern version of the experiment where Galileo Galilei (supposedly) dropped different iron spheres from the Tower of Pisa to show that they fell with the same acceleration. In the AEGIS experiment the equipment is a bit more sophisticated, but the principle is the same. The antihydrogen atom will be formed by combining excited positrons and antiproton in an antimatter trap. The reaction used in the experiment is



In this trap the antihydrogen atoms will be kept stable by strong magnetic fields before they are accelerated by an electric field. When they leave the acceleration area they will be

⁵Postironium, an unstable system consistent of an electron and a positron.

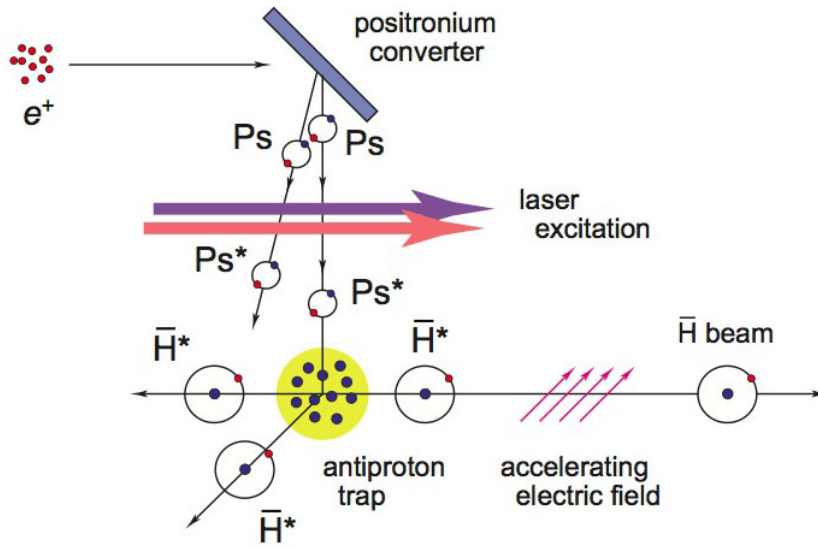


Figure 1.1: The experimental setup for the antihydrogen creation and acceleration step in the AEGIS experiment [1].

shot towards a detector. From the detected values a flight of path will be calculated and one will hopefully be able to measure the effect of gravity. In the AEGIS experiment the goal is to achieve a precision of 1% on the gravity measurement. To achieve this precision, about 1.3×10^5 antihydrogen atoms have to reach the detector. The experimental setup is shown in Figure 1.1.

In order for enough antimatter to reach the detector one has to make sure that the antihydrogen atoms are in fact being accelerated towards the detector by the electric field. For an electrostatic force to affect the neutral antihydrogen atom, there must be introduced a charge displacement in the atom. This induces a dipole where the negative antiproton acts as the negative pole and the positron is the positive pole. This is called polarization and it has a direction depending on where the positron is located. When the antihydrogen atoms are formed, they are created with positrons excited to many different energy levels. The resulting antihydrogen atoms will thus also have the positrons in many different energy levels and therefore in many different polarized states. If the antihydrogen atom is polarized in the wrong direction or not polarized at all, it will not accelerate towards the detector.

The antihydrogen atoms in the AEGIS experiment will have the positrons excited to high main quantum numbers (n). Atoms with highly excited electrons are called Rydberg atoms. In this experiment n is going to be between 30 and 40. This corresponds to a radius of about 50-85 nm and thus the dynamic of the single atom is nanoscience. The very large radius of Rydberg atoms results in very loosely bonded electrons, a fact stemming from the Coulomb interaction,

$$E = \frac{1}{4\pi\epsilon_0} \frac{Q_1 Q_2}{R}. \quad (1.2)$$

The low potential together with the fact that the energy levels get closer with higher n -levels make it easy for electrons to be ionized or shifted to other levels. The large radius also gives a possibility for large dipole moments of the Rydberg atom. In an external electric field a dipole will experience a shift in its energy. Electronic states with the electrons/positrons located along the field in the right direction will experience a lowering in energy. This is known as a Stark shift [30]. All these effects make Rydberg atoms "easy" to manipulate using laser pulses.

A laser pulse is an intense burst of coherent photons. In 1917 Einstein published a paper on stimulated emission giving the framework for the development of lasers [31]. In 1960 the first laser was invented [32] and technology has progressed since making it possible to create shorter bursts and shape the pulses. This progress has even made it possible to use lasers to control chemical reactions [33] [34].

The goal of this thesis has been to study if it will be possible to take the antihydrogen system from any of the initial states to a target state that has the correct polarization. It is possible to control the transitions of electrons using pulses and the challenge will be to find one that can do the right transitions in the right time frame.

1.4 Quantum control to control polarization

There has been developed numerous theoretical frameworks for finding an optimal pulse. In this work we use quantum control based on optimal control theory (OCT) to find a pulse to control the polarization of the antihydrogen. OCT is a mathematical technique applied to calculate the (optimal) control functions of a given equation of motion. OCT is today used in various engineering fields where you have a differential equation and an external parameter that influences the system. The basis of an OCT problem is that you have a functional where you want to maximize the outcome, and a variable that can be adjusted to find the best solution. In our case the functional depends on the optimizations, which are the population in the target state and the restriction on the field, the equation of motion which is the TDSE, and the variable which is the pulse. [35]

This type of quantum control is based on a closed learning loop where we have an initial guess on the pulse. Then we solve the TDSE forward in timesteps and see if we have reached the target state at the final time. If not, the final population will be used as a starting point for a backward propagation of the TDSE in time. The solutions in each time step for both the forward and backward propagations is used to calculate a new field for the next iteration (more detailed in Chapter 2). This will hopefully converge towards a pulse that optimizes the output. To ensure convergence, the initial guess for the pulse is important. For the iterations we need computational power and a fast iterative scheme is desirable.

The greatest problem with quantum control is that it does not necessarily find a pulse which is experimentally feasible. To account for this we need to put some restrictions on what pulses are allowed. This restriction can somewhat be applied in the equations, but it still does not guarantee a good pulse. Development in laser pulses has come a long

way, but there are still limitations in terms of signal-to-noise ratio and shaping. These limitations are things we need to take into account if we are to find an experimentally useful pulse. Another is the setup of the experiment. How will the strong magnetic field affect the energy levels? How much do we have to expose the system to our laser field and what kind of lasers do we have available for the system?

1.5 Outline and outlook

The goal of this thesis is to look at the chances for a multi-initial optimization to be applicable for the AEGIS project and see what limitations and requirements must be taken into account. To do this we use smaller systems that validly can be compared to the situation in the AEGIS project.

As the reader now hopefully has realised this thesis is a theoretical endeavour. It would not be purposeful to try out different pulses on real antihydrogen to try to find the correct one. In this work there have done simulations using Fortran and Matlab codes. Some of them are based on work done by former students in the group of optic and atomic physics at UiB, Lene Sælen and Raymond Nepestad. As an outline we will first go more in depth on the theory briefly touched upon in this chapter. It will also show the general iterative scheme for finding an optimal pulse as well as some variations you can apply. In this thesis we will be using atomic units, described in Appendix A, unless otherwise mentioned.

The first case will be a ten level asymmetric well system. Here we will study the general quantum control problem and see if we can optimize the transition from one state to another. Then we will expand this to two initial states and look on how this effects the optimization. From here we move over to a two dimensional (2D) hydrogen representation and look at some of the parameters that influence the optimization of an atom. In the 2D hydrogen study, we will try to find a pulse that pushes the electron to the electronic state that gives the highest dipole moment in the y-direction. Finally we will look into how a magnetic field influences the three dimensional(3D) atomic system and see if this promotes a different result than the 2D model when we try to optimize the polarization in the z-direction.

The background for this thesis is the AEGIS experiment, but quantum control can be utilized in many different areas. The target for the optimization can vary, and the only initial restriction is that it must be an hermitian operator to satisfy the quantum mechanical rules. By using quantum control to design pulses one may be able to control many atoms at the same time, making it more effective than the STM. This might be useful for nanotechnology to realize new applications. One possibility is to control the electronic states of quantum dots. A quantum dot can be simply described as an artificial atom where the potential is constructed. We can therefore make materials with energy-levels that suits our purpose. One purpose for the quantum dot is as a q-bit in the theorized quantum computer. If we are able to do this, we have really reached the possibility to create machines from atoms like Feynman foretold.

Chapter 2

Theory

This chapter will include some of the basic theory that this thesis builds on. In general the information is from [30], unless otherwise stated.

2.1 Optimal control theory

The optimizations in this thesis will be based on a mathematical framework called optimal control theory. Optimal control theory has its foundation in Bernoulli's¹ solution to the Brachystochrone problem². From his solution and onward to variation theory, the great breakthrough came in 1958 with the Pontryagin Maximum Principle which will be described below. Fuelled by the space race and optimizing of rocket trajectories the field developed and is today used in almost all engineering disciplines.

2.1.1 Theory

In [37] the basic problem of optimization is described as follows,

$$\dot{x}(t) = \mathbf{f}[\mathbf{x}(t), \mathbf{v}(t)]. \quad (2.1)$$

Here $x(t)$ is the system dynamics with an initial condition $x(t = 0) = x_0$ and a set of controls $v(t)$ in the vector space U . The objective is to find $\mathbf{u}(t)$ such that the total functional

$$J = J_1[\mathbf{x}(T)] + \int_0^T dt J_2[\mathbf{x}(t), \mathbf{v}(t)] \quad (2.2)$$

is maximized where J_1 represents the maximization of the outcome at the final time T , and J_2 is the restriction of the input. Depending on the system in equation (2.1) and

¹Johann Bernoulli(1667-1748).

²The Brachystochrone problem was formulated in 1696 and asked the reader to find the orbit that took the moveable point M under influence of its own weight from A to B in the shortest amount of time. The solution to the problem was found to be the cycloid [36].

the allowed controls, U , the found solution $\tilde{\mathbf{u}}(t)$ is not necessarily unique and there may exist other solutions. Since the goal is a maximization of J , it is natural to do a variation with respect to the control $\mathbf{u}(t)$. However, it is difficult to do the variation directly, so the functional J is replaced by

$$\tilde{J} = J - \int_0^T dt \lambda^\dagger(t) \{ \dot{\mathbf{x}}(t) - \mathbf{f}[\mathbf{x}(t), \mathbf{v}(t)] \}. \quad (2.3)$$

From equation (2.1) we have that the expression inside the curly brackets equals to zero, and the constrained problem has been transformed to an unconstrained one.

By using the new functional in the variation $\partial\tilde{J} = 0$ we get a set of equations and conditions for optimality, which are called *Pontryagin Maximum Principle* (PMP)

The theorem and complete proof can be found in [38]. *Theorem:* Suppose $\mathbf{u}(t) \in U$ and $\mathbf{x}(t)$ represent the optimal control and state trajectory for the optimal control problem described by 2.1 and 2.2 . Then there is an adjoint trajectory $\lambda(t)$ such that together $u(t)$ and $\lambda(t)$ satisfy

$$\dot{\mathbf{x}}(t) = \mathbf{f}[\mathbf{x}(t), \mathbf{u}(t)], \quad (2.4)$$

$$x(t=0) = x_0, \quad (2.5)$$

$$-\dot{\lambda}^\dagger(t) = \lambda^\dagger(t) \mathbf{f}_x[\mathbf{x}(t), \mathbf{u}(t)] + \nabla \mathbf{J}_2[\mathbf{x}(t), \mathbf{u}(t)], \quad (2.6)$$

$$\lambda^\dagger(t) = \nabla J_1[x(T)], \quad (2.7)$$

where f_x represents the matrix of partial derivatives

$$\mathbf{f}_x = \nabla \mathbf{f} = \left(\frac{\partial}{\partial \mathbf{x}_j} \mathbf{f}_i(\mathbf{x}, \mathbf{u}) \right).$$

For all t , $0 \leq t \leq T$, and all $\mathbf{v} \in \mathbf{U}$

$$H[\lambda(t), \mathbf{x}(t), \mathbf{v}(t)] \leq \mathbf{H}[\lambda(t), \mathbf{x}(t), \mathbf{u}(t)], \quad (2.8)$$

where H is the Hamiltonian

$$H[\lambda(t), \mathbf{x}(t), \mathbf{u}(t)] = \lambda^\dagger(t) \mathbf{f}[\mathbf{x}(t), \mathbf{u}(t)] + \nabla \mathbf{J}_2[\mathbf{x}(t), \mathbf{u}(t)]. \quad (2.9)$$

2.1.2 Classical example - the triangle problem

This example is taken from [37]. It is desired to draw a curve $x(t)$, $0 \leq t \leq T$, starting at $x(0) = 0$, whose slope at each point is no greater than 1 and attains maximum height at T . This is a simple problem, for it is clear that the solution is to select $x(t)$ as the straight line with slope equal to 1. However it shows the mechanics of the maximum principle.

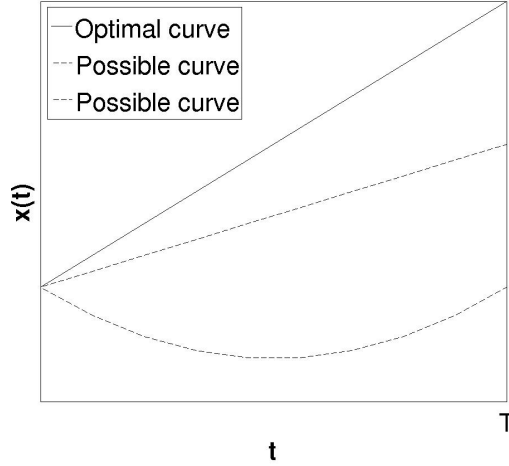


Figure 2.1: Possible and optimal solutions of the triangle problem.

The problem can be formulated in the following way,

$$\begin{aligned}\dot{x}(t) &= u(t), \\ x(0) &= 0, \\ u(t) &\leq 1, \\ J &= x(T).\end{aligned}$$

The objective is to maximize the height and the control to do so is the slope. In this problem we do not have any restrictions on u , such that $\nabla J_2 = 0$. We also have $f_x(x, u) = 0$ and therefore, the adjoint equation is

$$-\dot{\lambda}(t) = 0$$

The final condition is $\lambda(T) = 1$, since $J_1(x) = x$. Hence we get that $\lambda(t) = 1$. The Hamiltonian becomes

$$H = \lambda u = u$$

Thus to maximize the Hamiltonian, $u(t)$ needs to be as large as possible. From the constraint $u(t) \leq 1$ we see that we must have $u(t) = 1$ which agrees with the intuitive solution.

2.2 Quantum mechanics

From the previous section we saw that optimal control theory needs an equation of motion for the system. In quantum systems, Newton's equations are no longer valid, instead the dynamics are described by the *time dependent Schrödinger equation* (TDSE),

$$i \frac{\partial \Psi}{\partial t} = \hat{H} \Psi. \quad (2.10)$$

Here Ψ is the wavefunction of the system and \hat{H} is the hermitian ³ Hamilton operator (this Hamiltonian must not be confused with the one in equation (2.9)). We see that this equation can easily be written on the form in equation (2.1).

If the Hamilton operator does not explicitly include a time-part, the wavefunction can be separated into a time independent equation,

$$\Psi(\vec{r}, t) = \psi(\vec{r})T(t), \quad (2.11)$$

thus we have from equation (2.10)

$$i\frac{dT(t)/dt}{T(t)} = \frac{\hat{H}\psi(\vec{r})}{\psi(\vec{r})}. \quad (2.12)$$

The left side is only dependent on t and the right side is only dependent on \vec{r} . Both sides has to be equal to a constant E . This gives us two equations, one for $T(t)$ and one for $\psi(\vec{r})$.

The solution to

$$i\frac{dT(t)/dt}{T(t)} = E, \quad (2.13)$$

is

$$T(t) = Ce^{-iEt}. \quad (2.14)$$

The other equation

$$\hat{H}\psi(\vec{r}) = E\psi(\vec{r}), \quad (2.15)$$

is called *the time independent Schrödinger equation* (TISE) and is an eigenvalue problem. The solutions $\psi(\vec{r})$ are called stationary states while the constant E is the eigenvalue of the Hamiltonian and in most cases the energy of the system.

The total time dependent wavefunction Ψ can be described by a set of stationary basis functions ψ_i ,

$$\Psi(\vec{r}, t) = \sum_i c_i \psi_i(\vec{r}) e^{-iE_i t}. \quad (2.16)$$

Where the basis must meet the orthonormal requirement,

$$\int^{\tau} \psi_i^* \psi_j \partial\tau = \langle \psi_i | \psi_j \rangle^4 = \begin{cases} 1, & \text{if } i = j \\ 0, & \text{if } i \neq j \end{cases}. \quad (2.17)$$

Where τ represents the whole space where the functions are defined.

³A hermitan matrix is one that is self-conjugated, $H = H^*$.

⁴The notation with the angles is called Bra-ket notation and will be used from here in the thesis

In equation (2.16) c_i is the *development coefficient*. If we assume that the system is completely described by the function Ψ , with the energy spectrum E then the probability of the operator giving the outcome, E_i , is equal to $|c_i|^2$.

Generally we can say that the measurable outcome of an operator is one of the eigenvalues to the complete set of eigenstates. And the expectation value of the operator is

$$\langle F \rangle = \sum_i |c_i|^2 f_i. \quad (2.18)$$

Since $|c_i|^2$ is equal to the probability, c_i is called the probability amplitude and $\sum_i |c_i|^2 = 1$.

Let us go back to the Hamiltonian operator \hat{H} . For a particle in a potential the Hamiltonian consists of two parts, the kinetic energy and the potential energy.

$$\hat{H}(\vec{p}, \vec{r}) = \frac{\hat{p}^2}{2m} + V(\vec{r}). \quad (2.19)$$

Here $\vec{p} = i\nabla$ and represents the momentum of the particle and m is the mass of the particle. Using this, equation (2.10) turns into

$$i \frac{\partial \Psi}{\partial t} = \left[-\frac{1}{2m} \nabla^2 + V(\vec{r}) \right] \Psi. \quad (2.20)$$

Since the Hamiltonian is time independent we can use equation (2.15) and we get

$$-\frac{1}{2m} \nabla^2 \psi + V\psi(\vec{r}) = E\psi(\vec{r}), \quad (2.21)$$

and here E represents the total energy of the system.

If the potential is known the equation can be solved and we find the eigenstates (wavefunctions) and eigenvalues (energies) of the system. The nature of the potential determines if the solution is exactly or must be approximated.

2.2.1 One dimensional asymmetrical well

We show an example of solving the TISE using a potential from [35], the asymmetrical well, which is defined as follows,

$$V(x) = \frac{\omega_0^4}{64B} x^4 - \frac{\omega_0^2}{4} x^2 + \beta x^3. \quad (2.22)$$

The TISE becomes

$$\left[-\frac{d^2}{dx^2} + \frac{\omega_0^4}{64B} x^4 - \frac{\omega_0^2}{4} x^2 + \beta x^3 \right] \psi(\vec{r}) = E\psi(\vec{r}) \quad (2.23)$$

To solve this problem we need a basis set of orthonormal functions. For harmonic oscillators, *Hermite polynomials* are very useful. This is a large group of orthogonal polynomials and can be defined by:

$$H_n(x) = e^{x^2} \left(-\frac{d}{dx} \right)^n e^{-x^2}, \quad (2.24)$$

$$H_{n+1} = 2xH_n - 2nH_{n-1}, \quad (2.25)$$

$$H'_n = 2nH_{n-1}, \quad (2.26)$$

$$\int_{-\infty}^{\infty} H_n^2(x)e^{-x^2} dx = \sqrt{\pi}2^n n!, \quad (2.27)$$

$$\int_{-\infty}^{\infty} H_n(x)H_m(x)e^{-x^2} dx = 0(n \neq m). \quad (2.28)$$

The Hermite polynomials can be incorporated to the solutions through the following equation

$$\psi_n = \left(\frac{m}{\pi} \right)^{\frac{1}{4}} \frac{1}{\sqrt{2^n n!}} H_n(x) e^{-\frac{1}{2}x^2}. \quad (2.29)$$

Since we now can construct a basis set of a size k of our own choosing, we need to solve equation (2.15) for our potential to find the probability amplitudes c_n and the energies of the $n \in k$ lowest states. Solving large matrices are normally done by computers, which solves the eigenvalue problem using built in algorithms, like the Arnoldi method [39].

By solving the equation we find the energies and the eigenstates. For a basis set with $k = 100$, the ten lowest energy levels are listed in Table 2.1 while the scaled probability distribution for the 5 lowest states are shown in Figure 2.2.

Table 2.1: The energy of the ten lowest state in the asymmetrical well.

Basis state	Energy
ψ_1	-0.6206
ψ_2	-0.4638
ψ_3	0.0816
ψ_4	0.3941
ψ_5	0.9088
ψ_6	1.4762
ψ_7	2.1116
ψ_8	2.8012
ψ_9	3.5395
ψ_{10}	4.3216

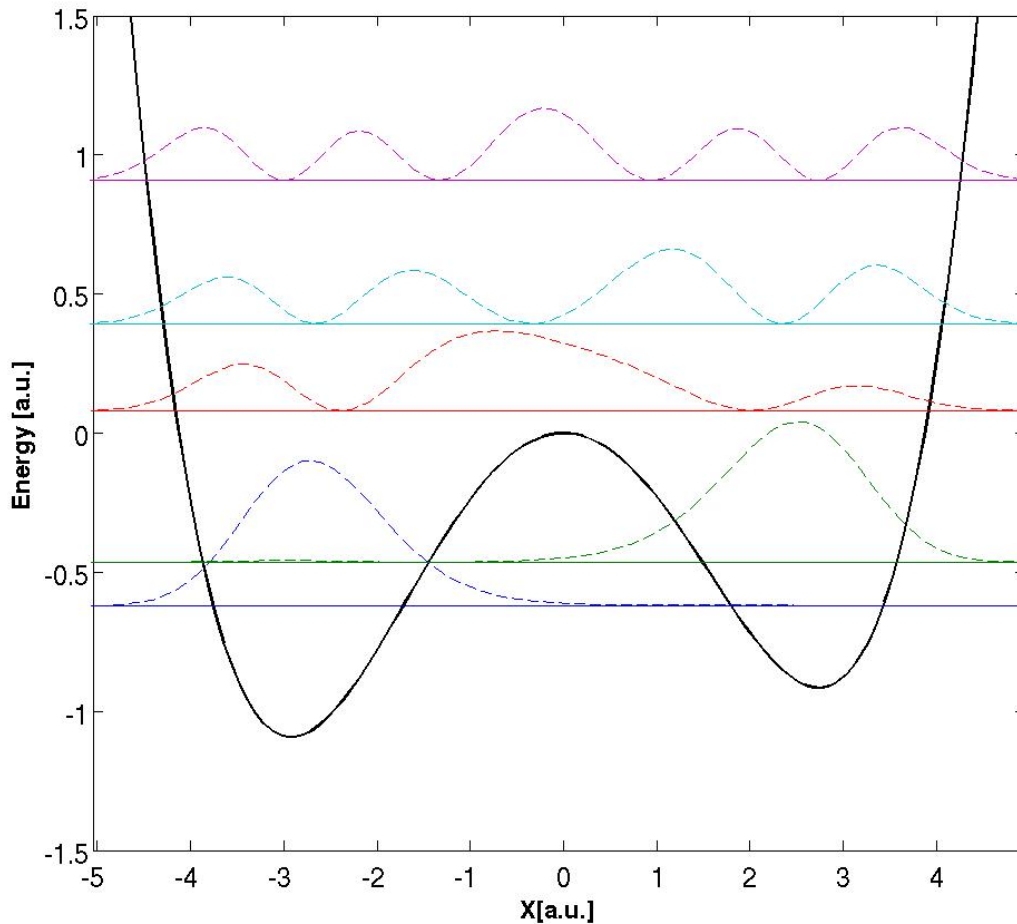


Figure 2.2: The asymmetric well with the density distribution of the 5 lowest states, scaled to the energies.

Figure 2.2 tells us that the lowest states are highly polarized in each of the wells. In the lowest state the particle is found exclusively in the lowest well to the left. While the second lowest state is almost entirely located in the well to the right. As we reach higher excited states the difference in the energies of the wells are of less importance and the states become less polarized. We see from the figure that already at state 5, the density is almost completely symmetrically distributed in the potential. We also notice the property of quantum mechanics called tunnelling. There is a small chance of finding the particle inside the "wall" of the well and if the wall is thin enough, the particle might be found on the other side. This is apparent for the second state; while the energy of state is lower than the potential barrier between the wells, there is a tiny chance of finding the particle in the left well. For the side walls however the potential grows so fast that the probability of finding them inside the wall is dying quickly.

We will return to the asymmetrical well and do more experimentation later.

2.3 Electromagnetic fields

In Maxwell's equations the electric, $\mathbf{E}(\mathbf{r},t)$ and magnetic field, $\mathbf{B}(\mathbf{r},t)$ are described by the following relations,

$$\mathbf{E}(\mathbf{r},t) = -\nabla\phi - \frac{\partial}{\partial t}\mathbf{A}(\mathbf{r},t), \quad (2.30)$$

$$\mathbf{B}(\mathbf{r},t) = \nabla \times \mathbf{A}(\mathbf{r},t), \quad (2.31)$$

where $\phi(\mathbf{r},t)$ is a scalar potential and $\mathbf{A}(\mathbf{r},t)$ is a vector potential.

These two potentials can be incorporated into the Schrödinger equation for a single particle with charge q and mass m .

Using the Coulomb gauge, $\nabla \cdot \mathbf{A} = 0$ and $\phi = 0$, we get the Hamiltonian,

$$\hat{H} = \frac{\mathbf{p}^2}{2m} - \frac{q}{m}\mathbf{p} \cdot \mathbf{A}(\mathbf{r},t) + \frac{q^2}{2m}\mathbf{A}(\mathbf{r},t)^2. \quad (2.32)$$

In a case where the field is used to probe the transitions within an atomic system, the wavelength will typically be much larger than the characteristic size of the atom. If the field intensity is not too high the spatial dependence of the field is negligible. This is often guaranteed with the quantitative restriction that $\mathbf{k} \cdot \mathbf{r} \ll 1$. This approximation is called the *dipole approximation*. This leads to a strictly time dependent vector potential and the Hamiltonian becomes,

$$\hat{H} = \frac{\mathbf{p}^2}{2m} - \frac{q}{m}\mathbf{p} \cdot \mathbf{A}(t) + \frac{q^2}{2m}\mathbf{A}(t)^2 + V(\mathbf{r}). \quad (2.33)$$

This can be transformed to a Hamiltonian with time dependence on the magnetic and electric field.

$$\hat{H} = \frac{\mathbf{p}^2}{2m} + \frac{q}{2m}\hat{\mathbf{L}} \cdot \mathbf{B}(t) + q\mathbf{r} \cdot \mathbf{E}(t) + V(\mathbf{r}) \quad (2.34)$$

Equation (2.34) is missing a diamagnetic term. The magnetic field scales with $1/cE$ and is usually neglected. However for strong magnetic fields it must be included. For a magnetic field in the z-direction, it is

$$\frac{q^2 B_z^2}{8m}(x^2 + y^2) \quad (2.35)$$

2.4 Quantum control

In a potential field the Hamiltonian will normally have the form as in equation (2.19), and we can call this \hat{H}_0 . However in quantum control we want to achieve a desired outcome and to do this we apply an arbitrary laser pulse to disturb the system. This can be seen as a perturbation to the Hamiltonian, and the new quantum mechanical operator turns into

$$\hat{H}_1 = \hat{H}_0 - \mu\epsilon(t). \quad (2.36)$$

Here H_0 represents the time independent operator, including the potential and the kinetic energy. μ is the external interaction, and ϵ is the temporal profile of the field(s). If the field is an electric field in the x-direction, $\mu = qx$ for a single particle, and a form of ϵ could be $\epsilon(t) = A_0 \cos(\omega t + \delta)$. We will now follow [35] to obtain the control equations.

The new pertubated TDSE becomes,

$$i \frac{\delta}{\delta t} \Psi = \left(\hat{H}_0 - \mu\epsilon(t) \right) \Psi. \quad (2.37)$$

Our goal is to find a laser pulse that drives the system from an initial condition to a final state that optimizes the expectation value of a target operator \hat{O} at the end of the laser interaction. However there is not certain that there is such a control and [40] and [41] has tried to determine some requirements the system must meet to be completely controllable.

The optimization of the expectation value can be expressed as,

$$\max_{\epsilon(t)} \underbrace{\langle \Psi(T) | \hat{O} | \Psi(T) \rangle}_{J_1}. \quad (2.38)$$

The only restriction on \hat{O} is that it has to be a Hermitian operator. Here $\Psi(T)$ is the solution in the final timestep to equation (2.37) with initial condition $\Psi(t=0) = \Phi_0$.

In addition to maximize J_1 , we minimize the fluency of the laser field. By this we want to reduce the efforts to obtain our desired outcome. The expression for this restriction is

$$J_2[\epsilon] = - \sum_j \int_0^T dt \alpha_j \epsilon_j^2(t), j = x, y. \quad (2.39)$$

Here α is the penalty factor, introduced to control the energy of the field. Together J_1 and J_2 forms a functional that we want to maximize,

$$J[\epsilon] = \langle \Psi(T) | \hat{O} | \Psi(T) \rangle - \sum_j \int_0^T dt \alpha_j \epsilon_j^2(t), j = x, y. \quad (2.40)$$

We see that the value of the penalty factor determines how much weight the limitation of the field has compared to the optimization of the expectation value. There is also the restriction that the wave function has to satisfy the TDSE. This is expressed through

$$J_3[\epsilon, \Psi, \chi] = -2Im \int_0^T dt \left\langle \chi(t) \left| \left(i\partial_t - \hat{H}(t) \right) \right| \Psi(t) \right\rangle, \quad (2.41)$$

where χ is an introduced Lagrange multiplier. Applying variation to the total functional with respect to all the variables ϵ , Ψ and χ we get

$$\delta_{\epsilon_k} J = \int_0^T d\tau \{-2\text{Im}\langle \chi(\tau) | \hat{\mu}_k | \Psi(\tau) \rangle - 2\alpha \epsilon_k(\tau)\} \delta \epsilon_k(\tau), \quad (2.42)$$

$$\delta_{\chi} J = -i \int_0^T d(\tau) \left\langle \left(i\partial_{\tau} - \hat{H}(\tau) \right) \Psi(\tau) | \delta \chi(\tau) \right\rangle, \quad (2.43)$$

$$\begin{aligned} \delta_{\Psi} J &= \left\langle \Psi(T) | \hat{O} | \delta \Psi(T) \right\rangle + i \int_0^T d\tau \left\langle \left(i\partial_{\tau} - \hat{H}(\tau) \right) \chi(\tau) | \delta \Psi(\tau) \right\rangle \\ &\quad - \langle \chi(T) | \delta \Psi(T) \rangle + \langle \chi(0) | \delta \Psi(0) \rangle. \end{aligned} \quad (2.44)$$

We want to find the extremum of the functional and therefore we set the variations equal to 0. This leads to some relations

$$\alpha_k \epsilon_k(t) = -\text{Im}\langle \chi(t) | \hat{\mu}_k | \Psi(t) \rangle, \quad k = x, y, \quad (2.45)$$

$$\left(i\partial_t - \hat{H}(t) \right) \Psi(r, t) = 0, \quad \Psi(r, 0) = \phi_i(r), \quad (2.46)$$

$$\left(i\partial_t - \hat{H}(t) \right) \chi(r, t) = i \left(\chi(r, t) - \hat{O} \Psi(r, t) \right) \delta(t - T), \quad (2.47)$$

$$\left(i\partial_t - \hat{H}(t) \right) \chi(r, t) = 0, \quad (2.48)$$

$$\chi(r, T) = \hat{O} \Psi(r, T). \quad (2.49)$$

These equations can be transformed to the more comprehensible forms

$$\epsilon(t) = -\frac{\text{Im}\langle \mu \Psi(t) | \chi(t) \rangle}{\alpha}, \quad (2.50)$$

$$i \frac{\partial}{\partial t} \Psi = \left(\hat{H}_0 - \epsilon(t) \mu \right) \Psi, \quad (2.51)$$

$$\Psi(0) = \Phi_0 \quad (2.52)$$

$$i \frac{\partial}{\partial t} \chi = \left(\hat{H}_0 - \epsilon(t) \mu \right) \chi, \quad (2.53)$$

$$\chi(T) = \hat{O} \Psi(T). \quad (2.54)$$

Ψ is the solution of the initial value problem, called the forward solution, while χ is the solution of the terminal value problem, called the backward solution.

The common way to solve the problem above is to split the time into a time grid and approximate the solution taking the field to be piecewise constant, $\epsilon(t_i) = u_i, t_i \in [0, T]$. Then we can iterate to find the optimal solution. For the first iteration we use an initial guess for the control. After the propagation, calculate the yield, $|\langle \Phi_t | \Psi^I(T) \rangle|^2$. There are many different possible algorithms to implement and solve the equations above and they all use a feedback cycle. The most common algorithm scheme is described below.

2.4.1 Algorithm scheme

The standard way to solve the control equations (2.50),(2.51),(2.52),(2.53) and (2.54) follows [42], which builds on [43]. In [44] a discussion on the convergence of the algorithm can be found.

In the first step of the algorithm you solve the Schrödinger forward using an initial field which we chose. A common choice is a constant field $\epsilon^0(t) = C$ where C can be equal to zero. However, it may be favourable to chose a field of considerable strength because if the $\left\| \hat{O}\Psi(T) \right\|$ is too low, the optimization tends to get stuck.

$$\text{step 0 : } \Psi^{(0)} \xrightarrow{\epsilon^{(0)}(t)} \Psi^{(0)}(T)$$

After the forward iteration we can use equation (2.54) to find the final state for the Lagrange multiplier, $\chi^{(0)}(T)$, and thus the starting point for the backward propagation. The propagation from $\chi^{(0)}(T)$ to $\chi^{(0)}(T - dt)$ is done with the field $\bar{\epsilon}^{(0)}(T)$, where $\chi^{(0)}(T)$ and $\Psi^{(0)}(T)$ are used in equation (2.50) to find it. The error the piecewise constant field introduces is reduced by choosing sufficiently small timesteps. In the next step from $\chi^{(0)}(T - dt)$ to $\chi^{(0)}(T - 2dt)$ the procedure is repeated, but instead with $\chi^{(0)}(T - dt)$ and $\Psi^{(0)}(T - dt)$ to calculate the new field value in equation (2.50). This proceeds until we reach $\chi^{(0)}(0)$. We either have to save the previous forward propagation or propagate backward with the old field in parallel to have access to the $\Psi^0(t)$ solutions. The step can be summarized as:

$$\text{step k : } \hat{O}\Psi^{(k)}(T) = \chi^{(k)}(T) \xrightarrow{\bar{\epsilon}^{(k)}(t)} \chi^{(k)}(0) \quad (2.55)$$

The last part of the zeroth step consists of setting $\Psi^{(1)}(0) = \phi_i$ and propagate $\Psi^{(0)}(0)$ forward with the field $\epsilon^{(1)}(t)$, determined by equation (2.50), where $\chi^{(0)}(t)$ and $\Psi^{(k+1)}(t)$ are used. Again we see that we either have to save the values of the backward propagation or propagate in parallel forward from $\chi^{(0)}$ to $\chi(T)$ with the old field $\bar{\epsilon}^{(k)}(t)$. The step can be summarized as

$$\phi_i = \Psi^{(k+1)}(0) \xrightarrow{\epsilon^{(k+1)}(t)} \Psi^{(k+1)}(T) \quad (2.56)$$

After the forward propagation the yield is calculated using equation (2.38). If the yield is high enough the optimization ends, if not the loop starts over again with equation (2.55).

The algorithm continues until it reaches an acceptable yield or a set number of iterations. The whole scheme can be summarized as follows:

$$\begin{array}{l} \text{step 0: } \Psi^{(0)}(0) \xrightarrow{\epsilon^{(0)}(t)} \Psi^{(0)}(T) \\ \text{step k: } \begin{array}{l} [\Psi^{(k)}(T) \xrightarrow{\epsilon^{(k)}(t)} \Psi^{(k)}(0)] \\ \hat{O}\Psi^{(k)}(T) = \chi^{(k)}(T) \xrightarrow{\bar{\epsilon}^{(k)}(t)} \chi^{(k)}(0) \\ [\chi^{(k)}(0) \xrightarrow{\epsilon^{(k)}(t)} \chi^{(k)}(T)] \\ \phi_i = \Psi^{(k+1)}(0) \xrightarrow{\epsilon^{(k+1)}(t)} \Psi^{(k+1)}(T). \end{array} \end{array}$$

The steps in the square brackets are the alternative parallel steps.

2.4.2 Laser field constraints

While there have been great advances in pulse shaping techniques, it is still not possible to create completely arbitrary pulses. To obtain more realistic pulses there have been developed restraints that can be applied to the laser pulse.

The most important factor that can be constrained are; limitation of the pulse energy, finite rise time of the electric field, fixing the laser fluence to a given value, spectral constraints on the laser field, phase-only shaping and a combination of the above mentioned.

The most common, and the two we will use in this work, are the before mentioned penalty factor and introducing an envelope by setting a time-dependence on α . Any additional restrictions on the field must be incorporated in the algorithm and this can lead to some problems. Some might not be general enough to be applicable in all situations, while others have poor convergence or strong dependence on the initial pulse.

To constrain the fluence to a certain value E_0 , the functional J_2 is altered to

$$\tilde{J}_2 = - \sum_{j=x,y} \alpha_j \left[\int_0^T dt \epsilon_j^2(t) - E_{0_j} \right]. \quad (2.57)$$

Here α_j is a time independent Lagrange multiplier. Instead of a specific value for this multiplier, a set value is prescribed E_{0_j} . When we then do variation with respect to α_j we get the new equation,

$$\int_0^T dt \epsilon_k^2(t) = E_{0_k}, k = x, y. \quad (2.58)$$

This leads to the need formula for the Lagrange multiplier which is incorporated in the algorithm and updated for each iteration

$$\alpha_k = \sqrt{\frac{\int_0^T dt [Im\langle \chi(t) | \hat{\mu}_k | \Psi(t) \rangle]^2}{E_{0_k}}}, k = x, y. \quad (2.59)$$

For the other filtering techniques a general filter is applied to the laser field for every iteration.

$$\epsilon_{out,j}(t) = \mathcal{G}[\epsilon_{in,j}(t)], j = x, y. \quad (2.60)$$

In principle, the filter can be any operator, but here we mention the most common (with $j = x, y$):

- Spectral filtering:

$$\epsilon_{out,j}(t) = \mathcal{F}^{-1}[f_j(\omega)\mathcal{F}[\epsilon_{in,j}(t)]], \quad (2.61)$$

where \mathcal{F} indicates as Fourier-transform and $f_j(\omega)$ is a frequency dependent function.

- Filtering in the time domain:

$$\epsilon_{out,j}(t) = h_j(t)\epsilon_{in,j}(t) \quad (2.62)$$

with the time-dependent envelope $h_j(t)$.

- Filtering for the phase-only optimization:

$$\begin{aligned} \epsilon_j(\omega) &= \mathcal{F}[\epsilon_{in,j}(t)], \\ \epsilon_{out,j}(t) &= \mathcal{F}^{-1} \left[A_j(\omega) \frac{\epsilon_j(\omega)}{|\epsilon_j(\omega)|} \right]. \end{aligned} \quad (2.63)$$

Where $A_j(\omega)$ is a given amplitude spectrum for the polarization j .

There exist other possible restrictions that can be allied and many are summarized in [35]. One promising example are piecewise constant control functions as demonstrated in [45].

Chapter 3

One Dimensional Asymmetrical Well

3.1 Single transition

We will now apply the algorithm we learned about in Chapter 2 to optimize a transition. We use the asymmetrical well discussed in Section 2.2.1 and shown in Figure 2.2. We will optimize the transition from the state that is centred on the lowest well to the state that is centred on the second well. From the previous chapter we have the basis and the energy of the ten lowest states as seen in 2.1. The coupling elements can be calculated from equation (2.34). We assume that there is only an electric field (the laser) that affects the system. This means that the coupling elements between the different electronic states is calculated as

$$\mu = \langle \Psi_i | X | \Psi_j \rangle \text{ for } i \neq j \in n \quad (3.1)$$

This leads to the matrix of coupling elements in Table 3.1

Table 3.1: The Coupling matrix for the ten lowest state in the asymmetrical well.

	1	2	3	4	5	6	7	8	9	10
1	-	-0.3921	-0.6382	0.3865	0.1414	0.0568	-0.0173	-0.0060	0.0017	-0.0005
2	-0.3921	-	-0.7037	-0.4630	0.2118	-0.0591	-0.0253	0.0060	0.00249	0.0005
3	-0.6382	-0.7037	-	1.7051	0.1593	0.2968	-0.0212	-0.0310	0.0021	-0.0027
4	0.3865	-0.4630	1.7051	-	-1.7862	0.0157	0.2416	0.0002	0.0228	-0.0001
5	0.1414	-0.2118	0.1593	1.7862	-	1.9498	-0.0197	0.2253	-0.0030	0.0198
6	-0.0568	-0.0591	-0.2968	0.0157	1.9498	-	2.0607	-0.0130	0.2136	-0.0020
7	0.0173	-0.0253	0.0212	0.2416	-0.0197	2.0607	-	2.1566	-0.0119	0.2060
8	-0.0060	-0.0060	-0.0310	0.0002	0.2253	-0.0130	2.1566	-	2.2420	-0.0106
9	0.0017	-0.0024	0.0021	0.0228	-0.0030	0.2136	-0.0119	2.2420	-	2.3201
10	-0.0005	0.0005	-0.0027	-0.0001	0.0198	-0.0020	0.2060	-0.0106	2.3201	-

The initial state is set to be the state laying in the lowest well with the lowest energy; $\phi_i = \Psi_1$, and the target state is set to be the first excited state which is laying in the

second well; $\phi_t = \Psi_2$. The operator we want to maximize the expectation value of is $\hat{O} = |\phi_t\rangle\langle\phi_t|$. For the initial propagation I have chosen a constant field, $\epsilon(t) = 0.01$ and for the following iterations there is a restriction on the form of the field that it has to follow a sine-mask,

$$\text{mask} = \sin(\pi \cdot /T)^2.$$

This will assure that the field will be zero at the start and the end. The other parameters for the simulation is summarized in Table 3.2. We see the initial and target state in Figure 3.1.

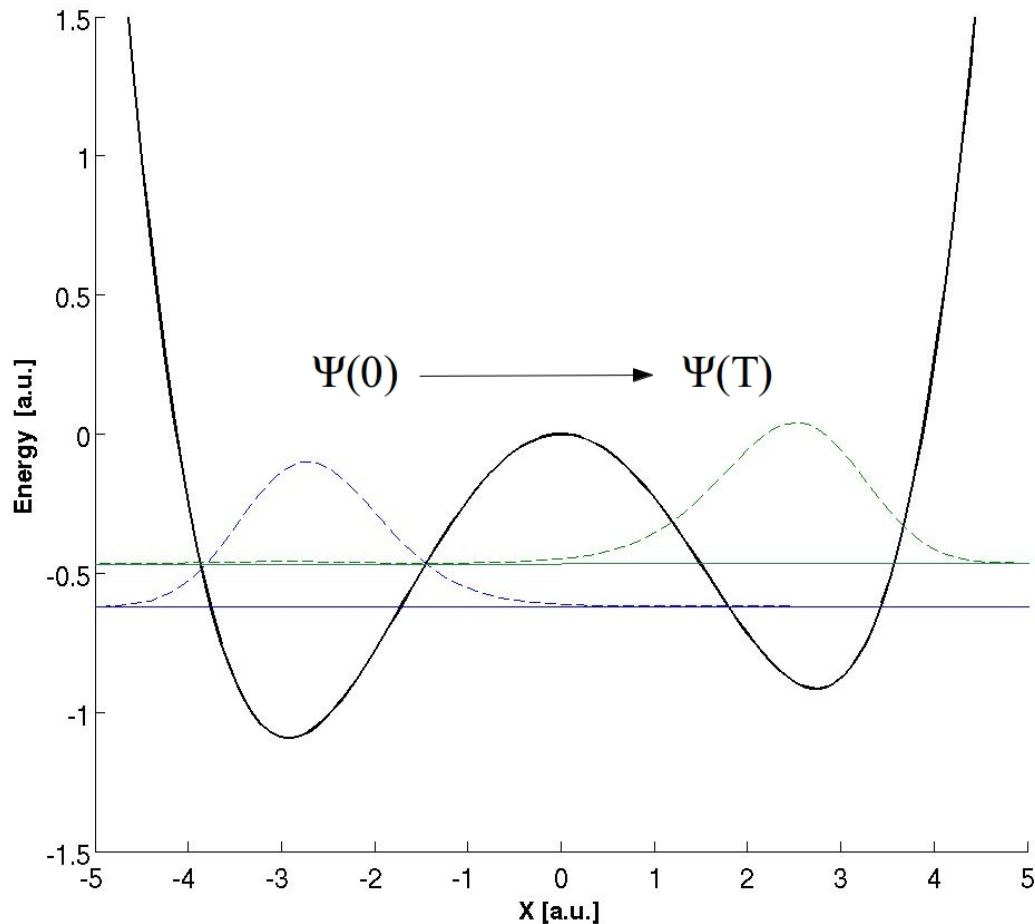


Figure 3.1: The two lowest energy states in the asymmetrical well with density distribution. The lowest state (with high population in the left well) is the initial state, ϕ_i , while the second lowest state (with high population in the right well) is the target state, ϕ_t .

The result of the optimization is shown in Table 3.3 and Figure 3.2. We see that it is very likely that we will be in the second well after the influence of the laser pulse. The density distribution was 96.63% in state 2 and 3.37% in state 1. The populations in the higher excited states were negligible.

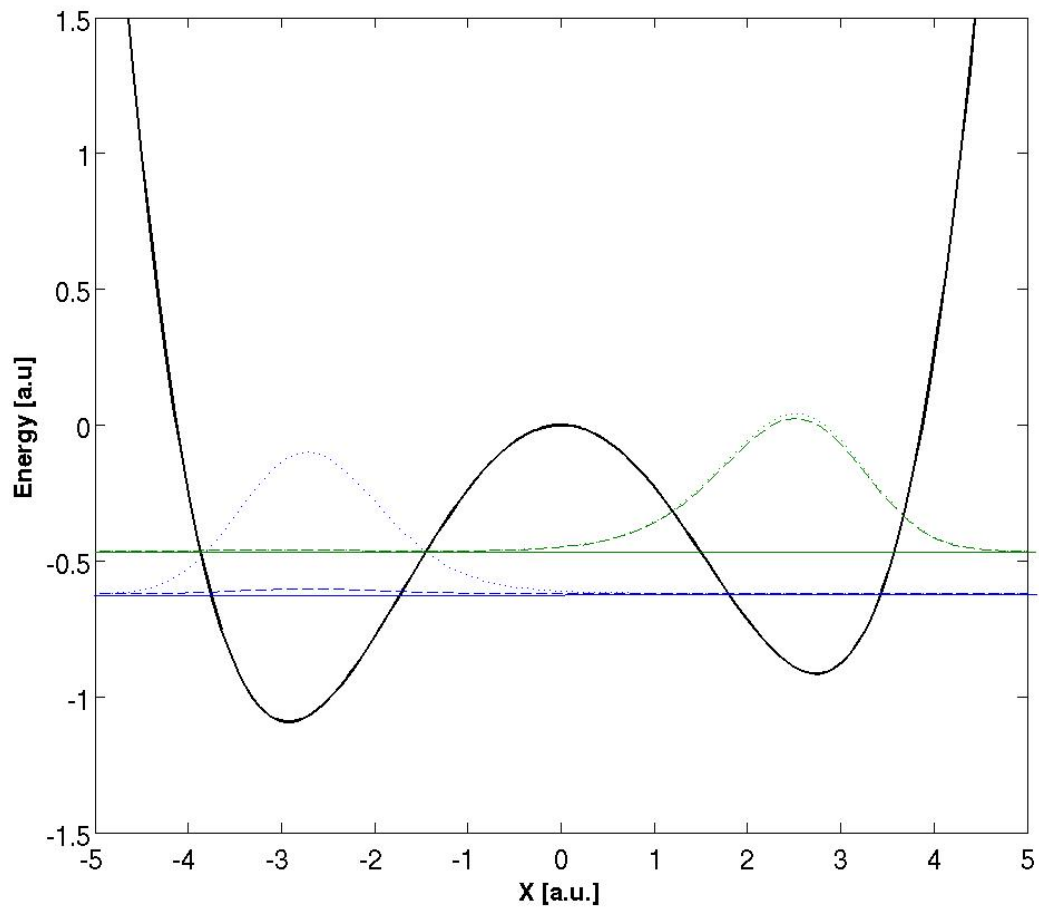


Figure 3.2: The final distribution between the states (dashed lines) and comparison to the original state and complete transition (dotted lines). The populations in the higher states were negligible.

Table 3.2: The simulation parameters for the single transition optimization.

Simulation parameter	Value
Basis size	10
Propagation time	2000 a.u.
Time step	0.05 a.u.
Initial field	Constant with amplitude 0.01
Max iterations	100
Yield	0.999
Mask	$\sin(\pi \cdot t/T)^2$
Penalty factor	10

Table 3.3: Results of the single transition optimization.

Parameter	Value
Yield	0.9663
Total functional	0.7789
Norm	1.0000
Final density in state 1	0.0337
Final density in state 2	0.9663

If we study the development of the yield in Figure 3.3 we notice that already after 10 iterations the increase in yield for each iteration is dramatically decreasing. After 20 iterations there is almost no change in the yield at all. The total functional (blue line) which we want to maximize, optimize the yield and minimize the value of the field, follows the same trend as the yield. This means that there are small changes in the field after 10 iterations as well.

The first and the final fields are shown in Figure 3.4.

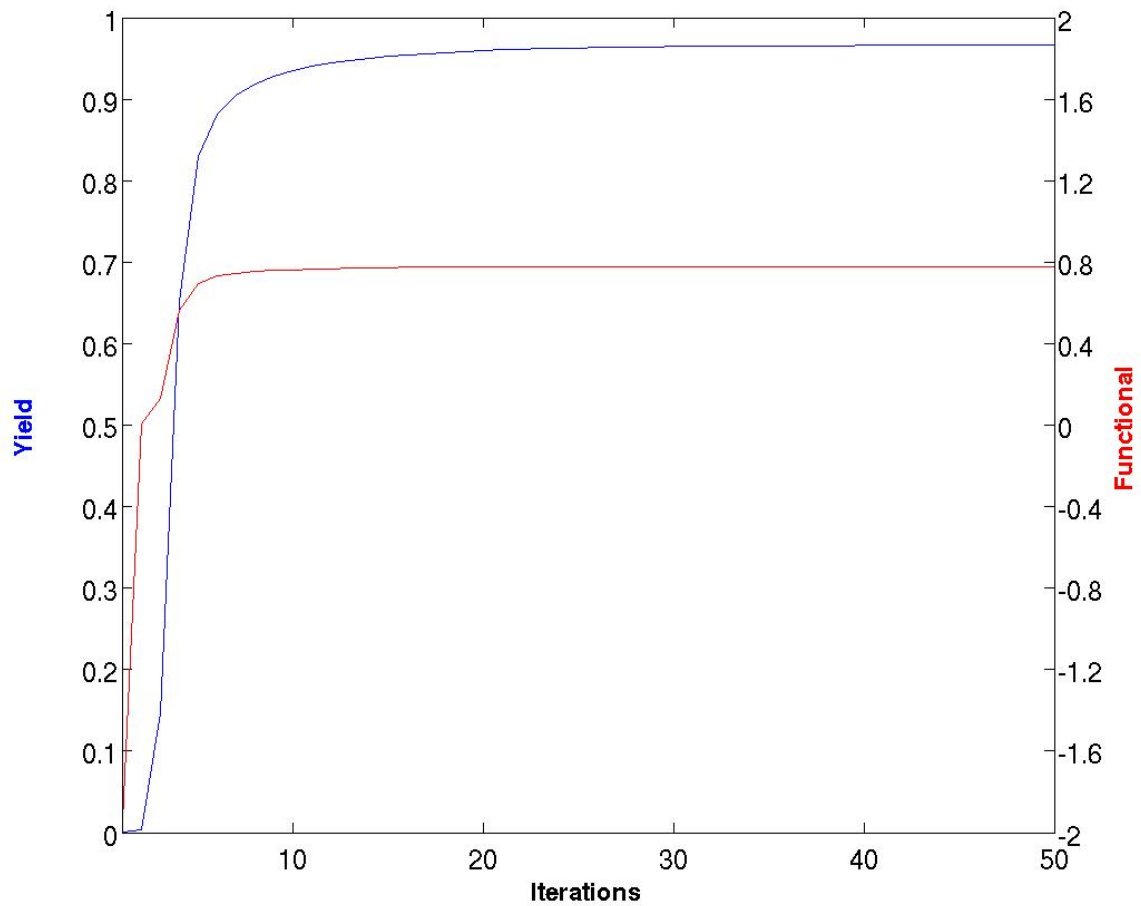


Figure 3.3: The development for the yield, in red, and the total functional, in blue, during the run. The optimization went on for 100 iteration, but is cut here to 50 due to limited increase after this point.

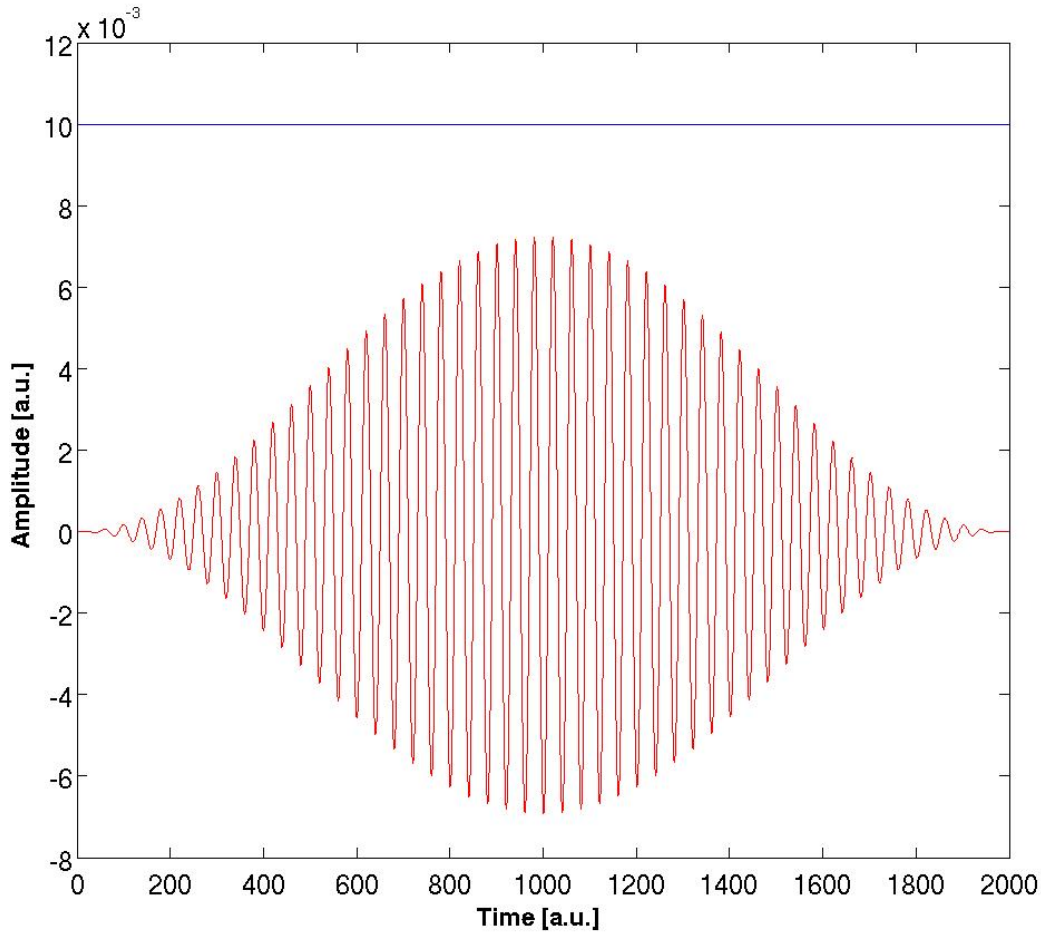


Figure 3.4: The initial guess for starting field in blue and the final optimized field in red.

From this optimization we see that we can quite effectively optimize single transitions, but what is the story for multiple initial states?

3.2 Multiple initial states

As mentioned in the introduction of the thesis, one of the greatest challenges of the AEGIS experiment is that we cannot control what state the antihydrogens will be in when they are created. This means that we want to find a pulse that takes the system to the correct final state independent of what the initial state is.

We want to test this by replicate the example from the previous section, but now optimize the transition from both state 1 and state 3 to state 2. However the two optimizations must be completely separated from each other. This is solved by extending the basis to 20 states, where 1 to 10 and 11 to 20 are identical. State 11 is the same as state 1, but in the state 3 to state 2 transition etc.. It follows that there is a coupling between the

10 first states and there is coupling between the 10 last states, but not between the two groups. The structure of the coupling matrix will look like in Table 3.4

Table 3.4: Structure of the coupling matrix for 2 initial states.

	1	2	...	10	11	12	...	20
1		-0.3921	...	-0.0005				
2	-0.3921		...	0.0005				
...				
10	-0.0005	0.0005	...					
11						-0.3921	...	-0.0005
12					-0.3921		...	0.0005
...				
20					-0.0005	0.0005	...	

Similarly the energies of the states will just be a duplication of the energy matrix of the single optimization.

The parameters for the simulation is summarized in Table 3.5 while the main results are summarized in Table 3.6. The final distribution of the density in the states is shown in Figure 3.5

Table 3.5: Simulation parameters for 2 initial states optimization.

Simulation parameter	Value
Basis size	20
Propagation time	2000
Time step	0.05
Initial field	Constant with amplitude 0.01
Max iterations	25
Yield	0.999
Mask	$\sin(\pi \cdot t/T)^2$
Penalty factor	20

Table 3.6: Result of the 2 initial state optimization.

Parameters	Value
Final yield	0.4522
Final functional	0.3104
Norm	1.0000
Final density in state 2	0.1521
Final density in state 12	0.3147
Final density in state 1	0.3458
Final density in state 13	0.0358

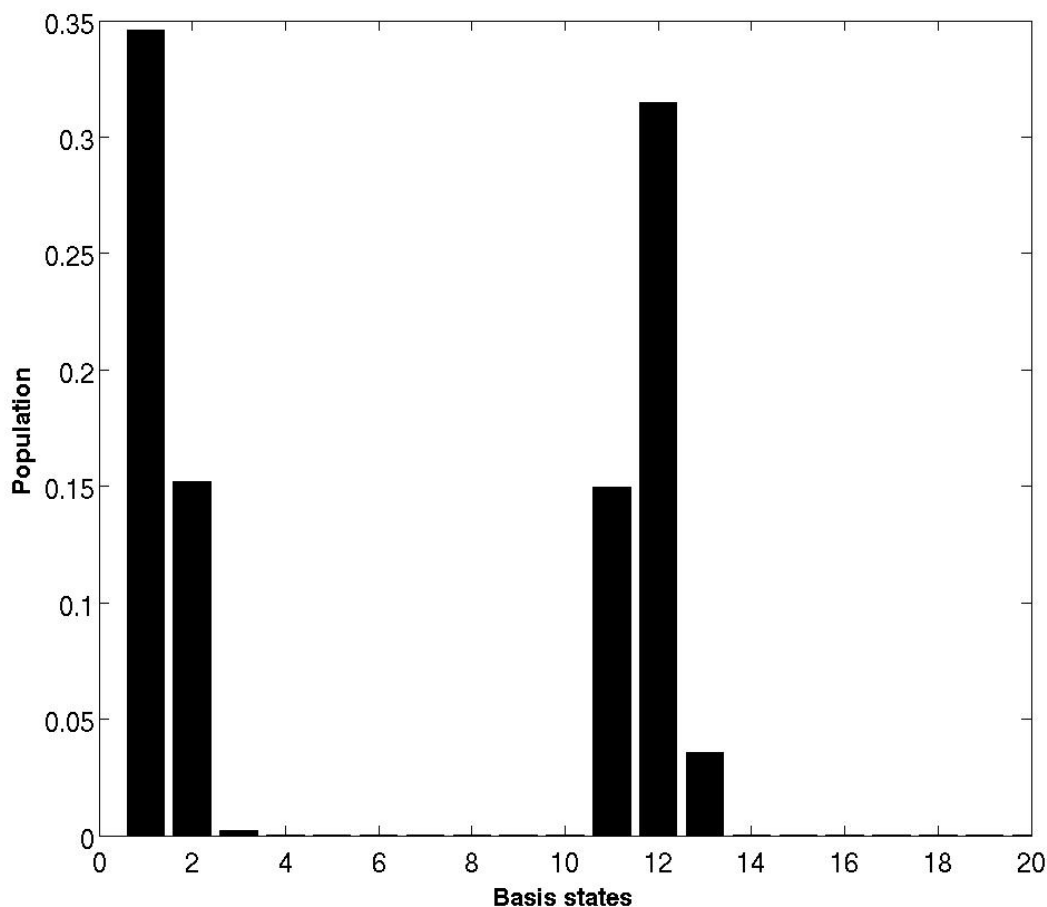


Figure 3.5: The density distribution between the twenty (really ten) states after 25 iterations.

Since the wavefunction is normalized, the maximum possible density in each of the two target states (2 and 12) is 0.5. This means that in reality the probability for each of the states being in the target state is twice of what is listed here. However the average probability of the electron being in the correct state is the sum of the two probabilities listed here. Thus if we have an even distribution of electrons in state 1 and 3 the field would take a random particle to the second state with a probability of 46.68%.

The interesting, but disappointing, fact is that this is no better than the single optimization. In the single transition the likelihood of finding the particle in the second well after the laser interaction is 96.63%. If half of the atoms is in the first state and half is in the third state then the average probability of a random particle to be in the second state is $0.9663 \cdot 0.5 = 0.48315$. Hence it is better to just optimize the 1 to 2 transition and not bother about the third state.

It should be pointed out that the optimization for the single transition went on for 100 iterations while this last one only was 25. However from looking at the development in figure 3.6 and figure 3.7 we see that already after 10 iterations the optimization has

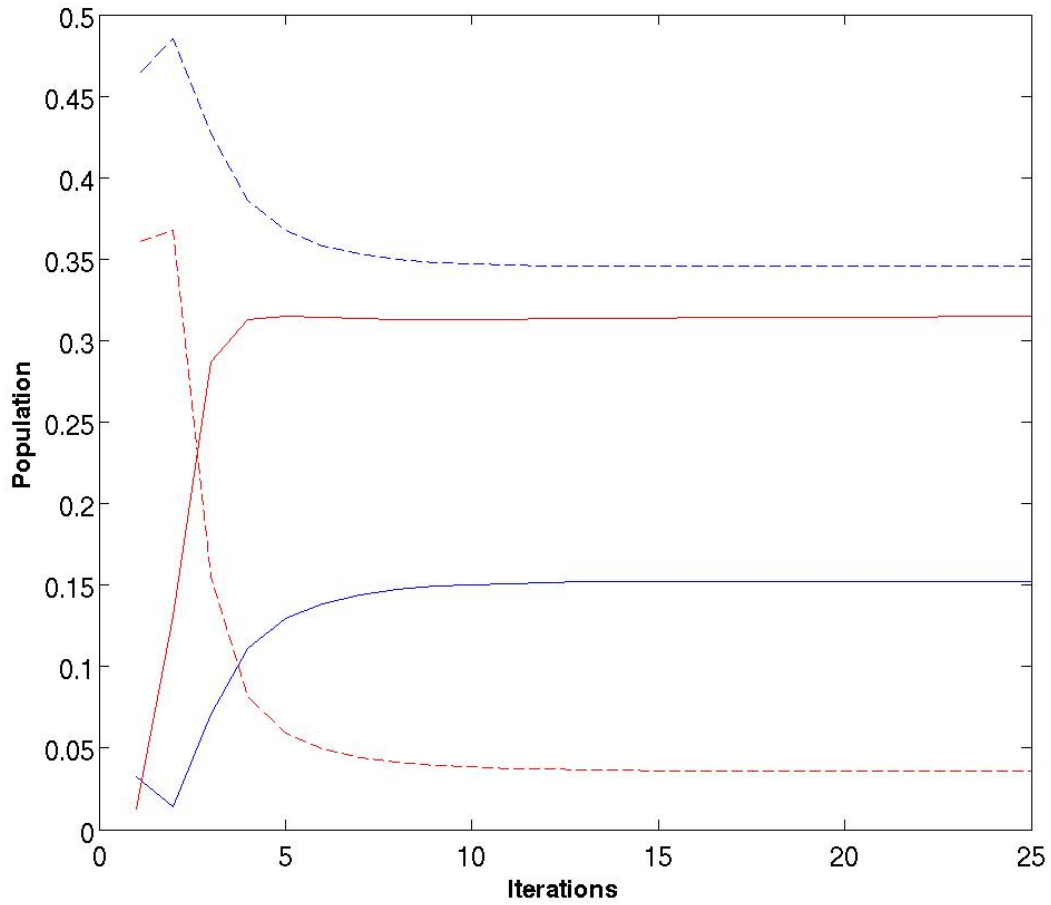


Figure 3.6: The development of the populations in the starting states and the target states. Target state 2 is blue while the initial state 1 is the blue stapled line. Similarly the red line is the target state 12(2), and the red stapled line is the initial state 13(3).

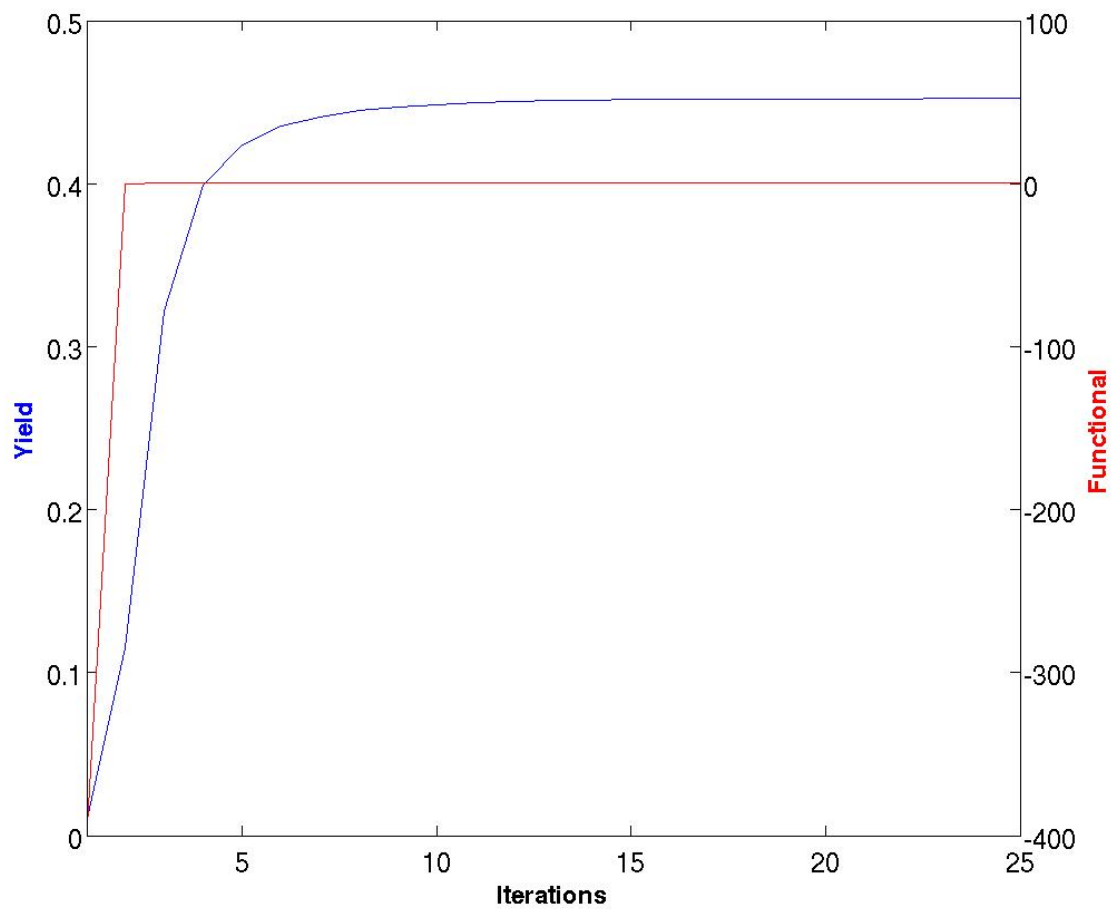


Figure 3.7: The development of the yield(red) and total functional(blue) for the two initial states optimization.

reached its peak so the difference is minimal. The penalty factor is also higher for this optimization, so all things considered, the two options are not very different. The final field for this optimization is shown in Figure 3.8.

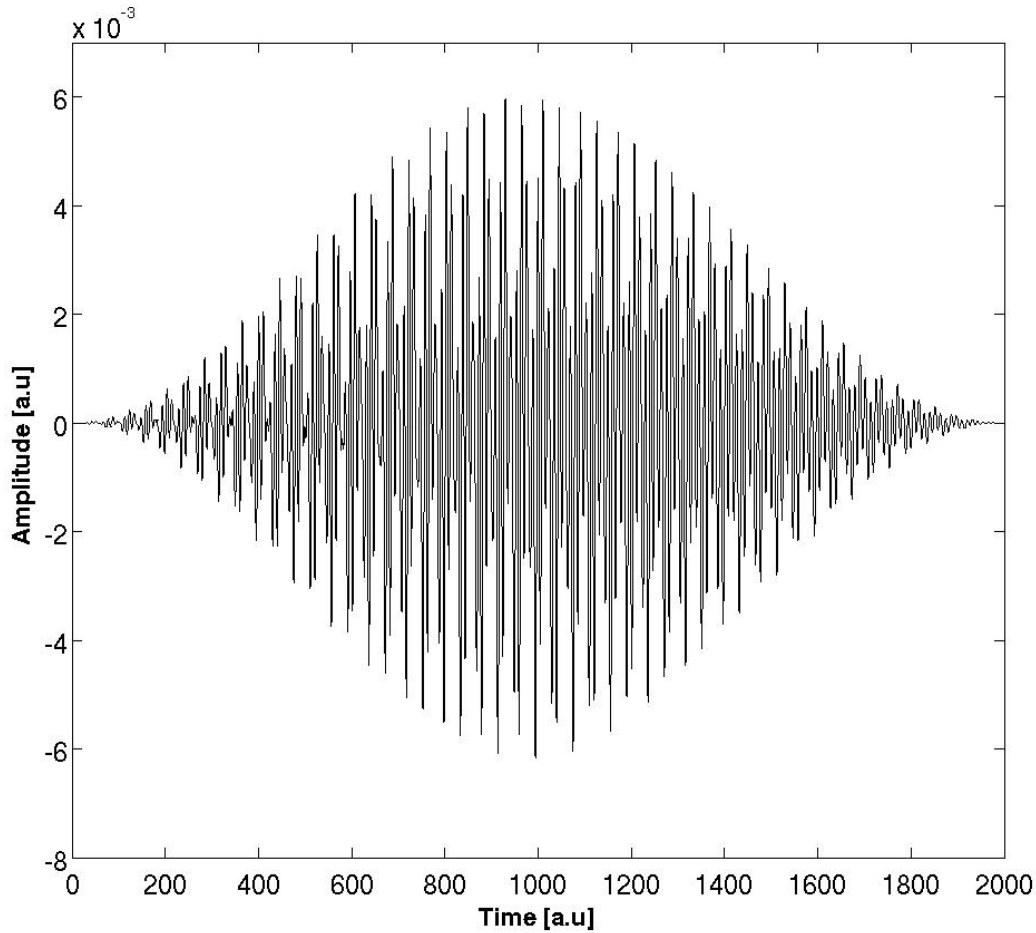


Figure 3.8: The optimal field for the transitions 1-2 and 3-2 found after 25 iterations.

From the previous exercise we concluded that a field optimization for two transitions is not better than focusing on just one of the transitions. This prompts the idea of a signal that consists of a train of two pulses, first the pulse for the 1 to 2 transition and then a pulse for the 3 to 2 transition. First we find the optimal pulse for the 3 to 2 transitions. This is done using the same simulation parameters as for the 1-2 optimization, listed in Table 3.2. The only difference is that now the initial state is the third state. The result of the optimization is shown in Table 3.7.

Table 3.7: The result of the 3 to 2 optimization.

Parameter	Value
Final yield	0.9813
Final Total functional	0.9071
Norm	1.0000
Final density in state 3	0.0187
Final density in state 2	0.9813

We see that the optimization for the 3 to 2 transition is even better than the first transition using the exact same run parameters. The field found is shown in Figure 3.9.

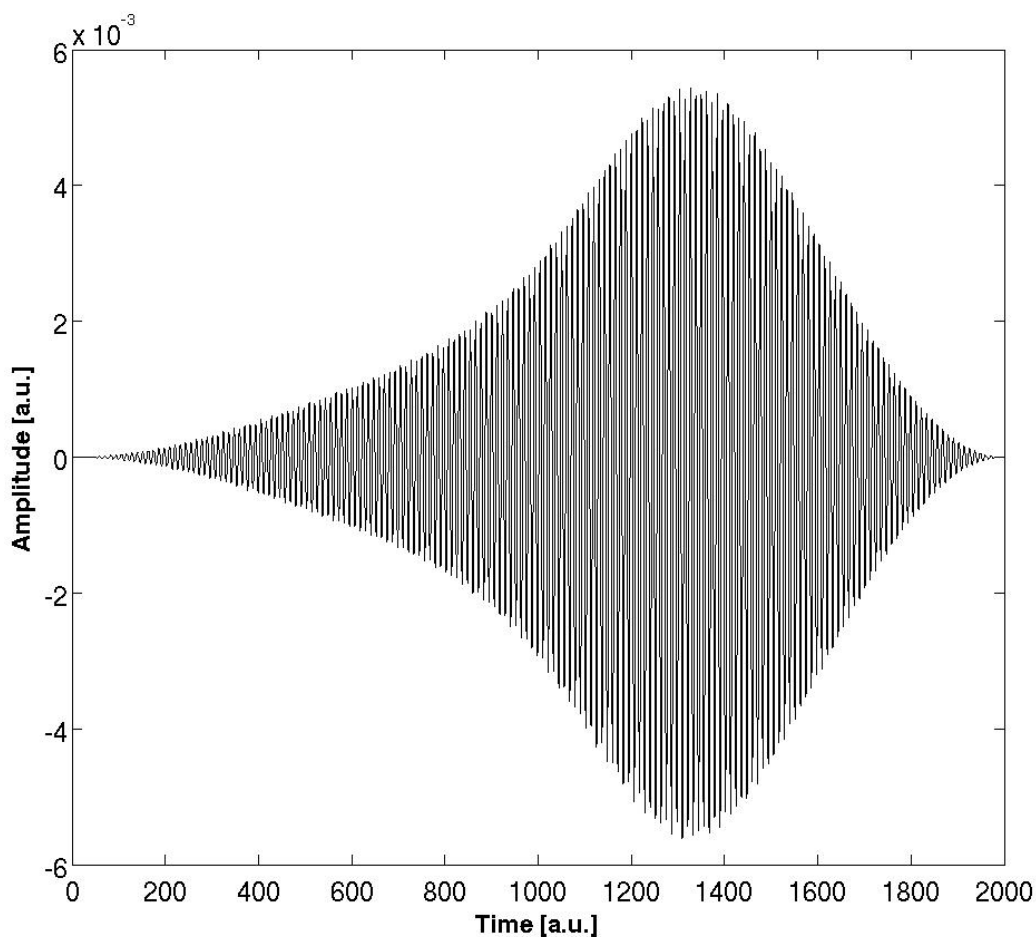


Figure 3.9: The optimized field for the 3 to 2 transition.

By creating a sequence of the two single transition optimization pulses, we get the pulse train shown in Figure 3.10. Hence, we have an initial field predefined by us lasting for 4000 atomic units of time. The field can then be used in the algorithm were the initial state is both the first state (1) and the third state (13).

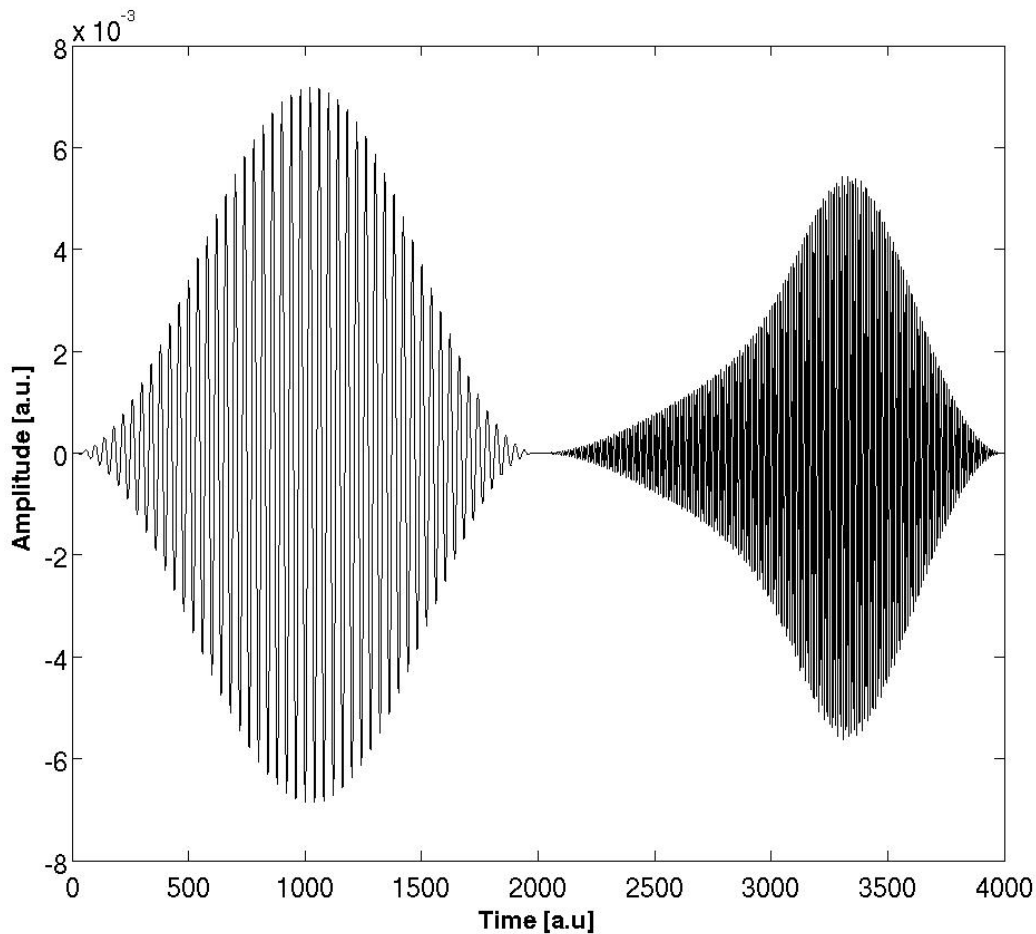


Figure 3.10: The string of pulses that first optimizes the 1 to 2 transition followed by the 3 to 2 optimization.

The results are shown in Table 3.8 and Figure 3.11. Notice first that the experiment does not yield the desired result. Combining two successful pulses is not any better than the single pulse. From the columns in Figure 3.11 we find that the second pulse has worked as designed. The population that was originally situated in state 13 (3) has been almost completely transferred to state 12 (2). However, we can also see that the first part of the optimization did not work as intended. The population that was originally situated in state 1 has been mostly transferred to the third state, while the goal was to populate the second state. The conclusion is that while the first pulse probably took the density from the first state to the second state, the second pulse probably both transferred the density in state 13 to 12 and the density in state 2 to state 3.

Table 3.8: The result after the puls train simulation.

Parameter	Value
Yield	0.2525
Total functional	-0.0065
Norm	1.0000
Density in state 1	0.0186
Density in state 2	0.0090
Density in state 3	0.4724
Density in state 11	0.0000
Density in state 12	0.4889
Density in state 13	0.0093

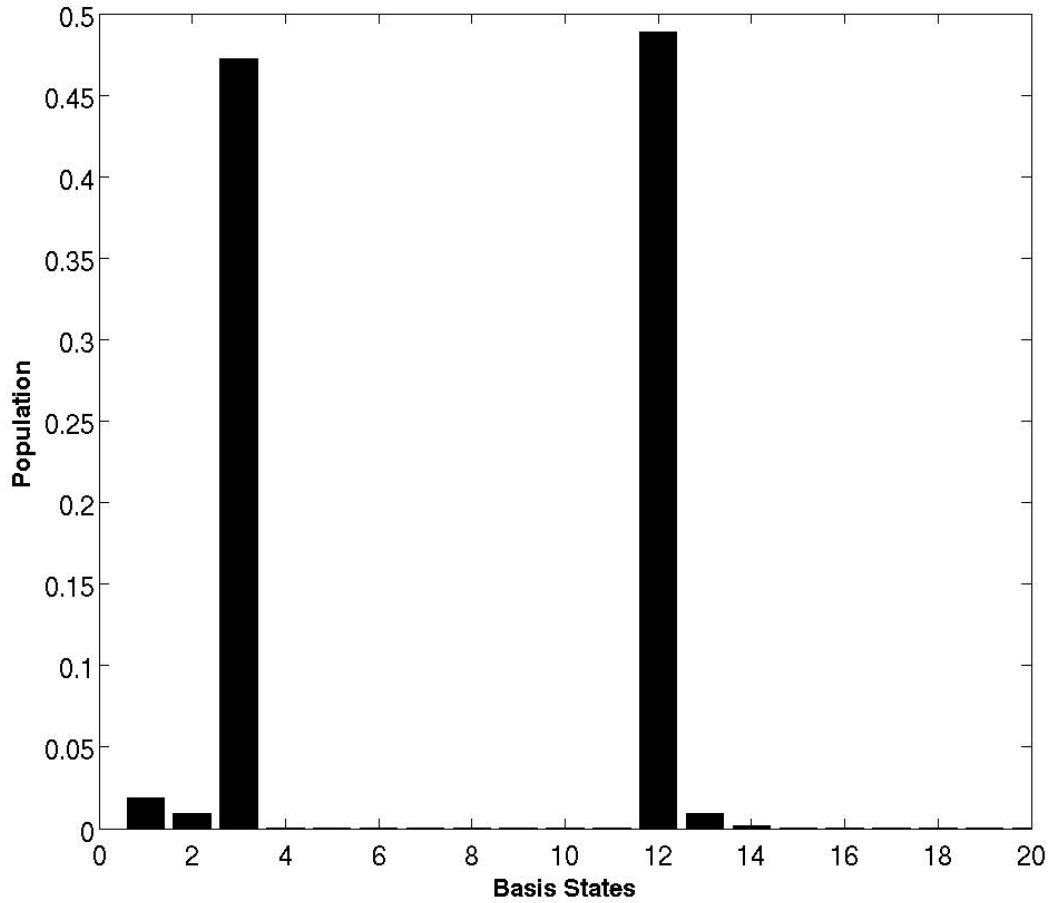


Figure 3.11: The distribution of the population after the pulsetrain has affected the system

3.3 Summary

The conclusion of this Chapter is that neither of the possible setups are optimal for multiple initial states. It seems that every solution is stuck in a distribution that is close to a 50% probability of finding the particle in the correct state. While it seems certain that the pulse train that the optimization for 3 to 2 also optimizes the 2 to 3 transition it is less conclusive for the single pulse. However, the field looks more complicated and it is reasonable to believe that the problem also is prominent here, but the field secures a more even distribution between the states. A thing worth noting is that more initial states probably will lead to more complicated pulse shapes, which is an experimental limiting factor. In the next chapter we will look more into what factors that affects how successful an optimization is.

Chapter 4

Two Dimensional Hydrogen Atom

From the asymmetrical well, we move on to the two dimensional (2D) Coulomb problem. This chapter explains and portrays some of the aspects that we also will encounter in the three dimensional hydrogen atom, but here we can address them in a simple setting. The derivation of the wavefunction is found in [30] and [46]

4.1 Polar coordinates and separation of variables

For the 2D hydrogen atom, the electron is only located in the xy-plane at a distance from the core in the center. The potential energy in the Hamilton will be equal to the Coulomb potential

$$V(r) = -\frac{1}{r}, \quad (4.1)$$

while the kinetic term only is considered for the electron,

$$-\frac{1}{2}\nabla^2 = -\frac{1}{2}\left(\frac{\partial^2}{\partial x^2} + \frac{\partial^2}{\partial y^2}\right). \quad (4.2)$$

To simplify our Hamilton we use polar coordinates to transform the Laplace operator

$$\begin{aligned} x &= r \sin \phi, \\ y &= r \cos \phi. \end{aligned} \quad (4.3)$$

The inverse transformation is

$$\begin{aligned} r &= \sqrt{x^2 + y^2}, \quad r \in [0, \infty), \\ \phi &= \tan^{-1} \frac{x}{y}, \quad \phi \in [0, 2\pi]. \end{aligned} \quad (4.4)$$

the derivatives now turns to

$$\begin{aligned}\frac{\partial}{\partial x} &= \sin \phi \frac{\partial}{\partial r} + \frac{\cos \phi}{r} \frac{\partial}{\partial \phi}, \\ \frac{\partial}{\partial y} &= \cos \phi \frac{\partial}{\partial r} - \frac{\sin \phi}{r} \frac{\partial}{\partial \phi}.\end{aligned}\quad (4.5)$$

By algebraic transformation we find the Laplace operator given in the new coordinates

$$\nabla^2 = \frac{\partial^2}{\partial r^2} + \frac{1}{r} \frac{\partial}{\partial r} + \frac{1}{r^2} \frac{\partial^2}{\partial \phi^2}.\quad (4.6)$$

The general time-independent Schrödinger equation is expressed in polar coordinates as

$$\left(-\frac{1}{2}\nabla^2 + V\right)\Psi(\mathbf{r}) = -\frac{1}{2}\left(\frac{\partial^2}{\partial r^2} + \frac{1}{r}\frac{\partial}{\partial r} + \frac{1}{r^2}\frac{\partial^2}{\partial \phi^2}\right)\Psi(\mathbf{r}) + V(r)\Psi(\mathbf{r}) = E\Psi(\mathbf{r}).\quad (4.7)$$

The 2-dimensional squared angular momentum is identified as

$$\hat{L}_{2D}^2 = -\frac{\partial^2}{\partial \phi^2}.\quad (4.8)$$

We now introduce the Coulomb potential from equation (4.1) to the Schrödinger equation,

$$-\frac{1}{2}\left(\frac{\partial^2}{\partial r^2} + \frac{1}{r}\frac{\partial}{\partial r} + \frac{1}{r^2}\frac{\partial^2}{\partial \phi^2} + \frac{2}{r}\right)\Psi(\mathbf{r}) = E\Psi(\mathbf{r}).\quad (4.9)$$

This equation can be solved by separation of variables. We write the wavefunction as a product of a radial part and a angular part. This yields,

$$\Psi(\mathbf{r}) = R(r)\Phi(\phi).\quad (4.10)$$

By examining equation (4.9), we see that it is possible to separate the equation in to two parts dependent on each own variable. These two parts must be equal to a constant,

$$\frac{r^2}{R(r)}\left(\frac{\partial^2}{\partial r^2} + \frac{1}{r}\frac{\partial}{\partial r} + \frac{2}{r} + 2E\right)R(r) = -\frac{1}{\Phi(\phi)}\frac{\partial^2}{\partial \phi^2}\Phi(\phi) = m^2.\quad (4.11)$$

Thus we have two equations that can be solved separately. The angular part has the solution,

$$\Phi(\phi) = \frac{1}{\sqrt{2\pi}}e^{im\phi}.\quad (4.12)$$

The angular function has to fulfill the requirement to be similar after a full rotation to be physical viable. This can be expressed as

$$e^{im\phi} = e^{im(\phi+2\pi)}. \quad (4.13)$$

This holds true when m is an integer: $m = 0, \pm 1, \pm 2, \dots$

The radial equation which is on the form

$$-\frac{1}{2} \left(\frac{\partial^2}{\partial r^2} + \frac{1}{r} \frac{\partial}{\partial r} - \frac{m^2}{r^2} \right) R(r) = ER(r), \quad (4.14)$$

is solved by introducing an auxiliary function $u(r)$ which has the relation $R(r) = r^{-\frac{1}{2}}u(r)$. By substituting for $R(r)$ and differentiating, we get the following equation for $u(r)$,

$$-\frac{1}{2} \left(\frac{\partial^2}{\partial r^2} + \frac{2}{r} - \frac{m^2 - \frac{1}{4}}{r^2} \right) u(r) = Eu(r). \quad (4.15)$$

To simplify, the *dimensionless coordinate*, ρ , is introduced with the relation

$$\rho = 2\epsilon r, \quad (4.16)$$

where

$$E = -\frac{1}{2}\epsilon^2. \quad (4.17)$$

By using this in equation (4.15) we get

$$\left(\frac{\partial^2}{\partial \rho^2} + \frac{1}{\epsilon \rho} - \frac{m^2 - \frac{1}{4}}{\rho^2} - \frac{1}{4} \right) u(\rho) = 0. \quad (4.18)$$

When ρ goes to infinity the only surviving terms of equation are

$$\frac{\partial^2 u(\rho)}{\partial \rho^2} \approx \frac{1}{4}u(\rho). \quad (4.19)$$

This has the solutions $e^{\pm\rho/2}$. We need a solution that does not go toward infinity, namely $e^{-\rho/2}$. From this we will try solutions on the form $u(\rho) = e^{-\rho/2}\nu(\rho)$. Inserting this into equation (4.18) and differentiating we get,

$$\left(\frac{\partial^2}{\partial \rho^2} - \frac{\partial}{\partial \rho} + \frac{1}{\epsilon \rho} - \frac{m^2 - \frac{1}{4}}{\rho^2} \right) \nu(\rho) = 0. \quad (4.20)$$

We solve by doing a series expansion of $\nu(\rho)$. Omitting details, the solution is

$$\nu(\rho) = \sum_{j=0}^{\infty} a_o \frac{|m| + j - n}{j(2|m| + j)} \rho^{|m| + \frac{1}{2} + j}, \quad (4.21)$$

where a_o is the normalization constant. To simplify the equation, $n = \frac{1}{\epsilon} + \frac{1}{2}$ has been introduced.

The problem with this solution is that it diverges for $\rho > 1$. To avoid this, it is required that the series terminates after a finite numbers of terms, while keeping at least one. This is achieved if $n = |m| + n_r, n_r = 1, 2, \dots$. We see that $|m| < n$.

Finally the total radial solution become; $R(\rho) = r^{-\frac{1}{2}} e^{-\frac{\rho}{2}} \nu(\rho)$,

$$R_{n,m}(\rho) = e^{-\frac{\rho}{2}} \sum_{j=0}^{N(n)} a_o \frac{|m| + j - n}{j(2|m| + j)} \rho^{|m| + j}, \quad (4.22)$$

with quantum numbers $n = 1, 2, 3, \dots$ and $|m| = 0, 1, 2, \dots, n - 1$. By this definition of n and equation (4.17) we find an expression for the energy

$$E_n = -\frac{1}{2} \epsilon^2 = -\frac{1}{2(n - \frac{1}{2})^2}. \quad (4.23)$$

However we will not use the power series solution, but instead realise that equation (4.15) is the Whittaker's equation [47]. The solutions are in form of Whittaker functions,

$$u(\rho) = e^{-\frac{\rho}{2}} \rho^{|m| + \frac{1}{2}} M \left(|m| - \frac{1}{\epsilon} + \frac{1}{2}, 2|m| + 1, \rho \right). \quad (4.24)$$

Since $n = \frac{1}{\epsilon} + \frac{1}{2}$, the first part of the argument is always less or equal to zero. The Whittaker's functions can then be written in terms of the associated Laguerre polynomials,

$$M(|m| - n + 1, 2|m| + 1, \rho) = CL_{n-|m|-1}^{2|m|}(\rho). \quad (4.25)$$

The radial function $R(\rho) = r^{-\frac{1}{2}} u(\rho)$, becomes

$$R_{n|m|}(\rho) = N_{n|m|} e^{-\frac{\rho}{2}} \rho^{|m|} L_{n-|m|-1}^{2|m|}, \quad (4.26)$$

where $N_{n|m|}$ is the normalization constant.

We write the total wavefunction to the Coloumb potential as a product of the angular solution and the radial solution

$$\Psi_{n,m}(\mathbf{r}) = N_{n|m|} e^{-\frac{\rho}{2}} \rho^{|m|} L_{n-|m|-1}^{2|m|} \frac{1}{\sqrt{2\pi}} e^{im\phi}, \quad (4.27)$$

with energy levels

$$E_n = -\frac{1}{2(n - \frac{1}{2})^2}. \quad (4.28)$$

We realize that m does not affect the energy levels which is comparable to the 3-dimensional hydrogen atom, where different l -quantum numbers does not affect the energy. This is because all the potential is only dependent on the distance between the electron and the core. The resulting eigenstates are all symmetrical and the angle is not affecting the potential at all.

4.2 Optimization example for $n=5$

We apply the solutions from the previous discussion, to an physical example where we will do a transition optimization.

We choose a hydrogen atom with only the $n = 5$ level available. In a real hydrogen atom there would be other energy levels available that would also been affected by the electric field. However if we restrict the pulse fluency, the Stark effect has less impact and the n -levels would not be mixed. So by restricting the field we can assume that electrons in the $n=5$ level will stay there and we diminish there error of excluding other energy-levels.

With $n = 5$, we have $m = -4, \dots, 0, \dots, 4$ giving a total of 9 basis functions. From equation (4.28) we have that the energy levels are degenerated with value $E = -0.0247$. The quantum numbers and energy of the system is summarized in Table B.1 in Appendix A.

We use equation (4.26) to calculate the radial wavefunction for our basis. We set the maximum radius for where we calculate the wavefunction to 75a.u. Outside this radius the wavefunction is set to zero. The radial distribution is shown in Figure 4.1.

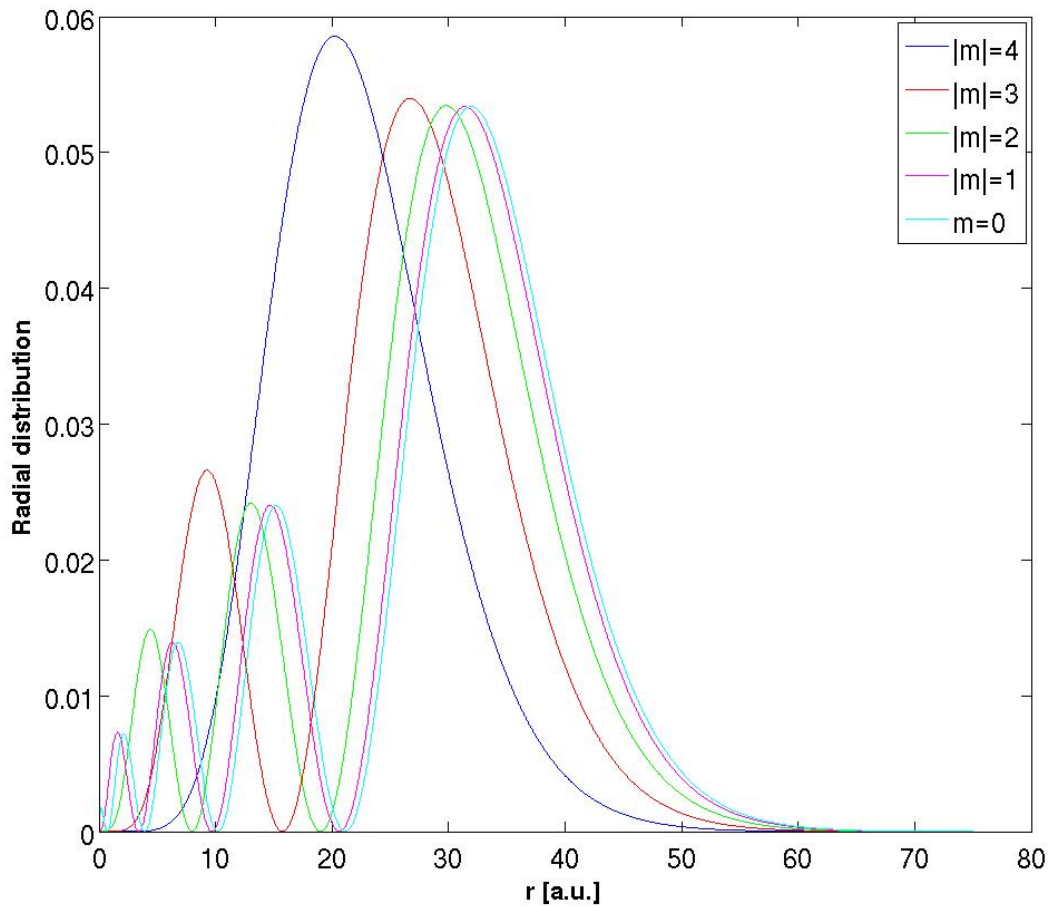


Figure 4.1: The radial distribution functions for the different quantum numbers, $n=5$ and $|m|=0, \dots, 4$.

Since the radial distribution only takes the absolute value of the m -quantum number, the radial distribution will be equal for the same integer. It is also worth noting that the radial distribution follows the rule of $n - m - 1$ nodal planes, as in the figure $|m| = 4$ (in blue) has no radial nodes. We see that the radial functions die before reaching 75 so this is an acceptable cut off distance. Finally we add the angular part of the solution, which is described in equation 4.12.

By including the angular parts we have the complete wave functions. In Figure 4.2 the real parts of the wavefunctions are shown for the different m -values.

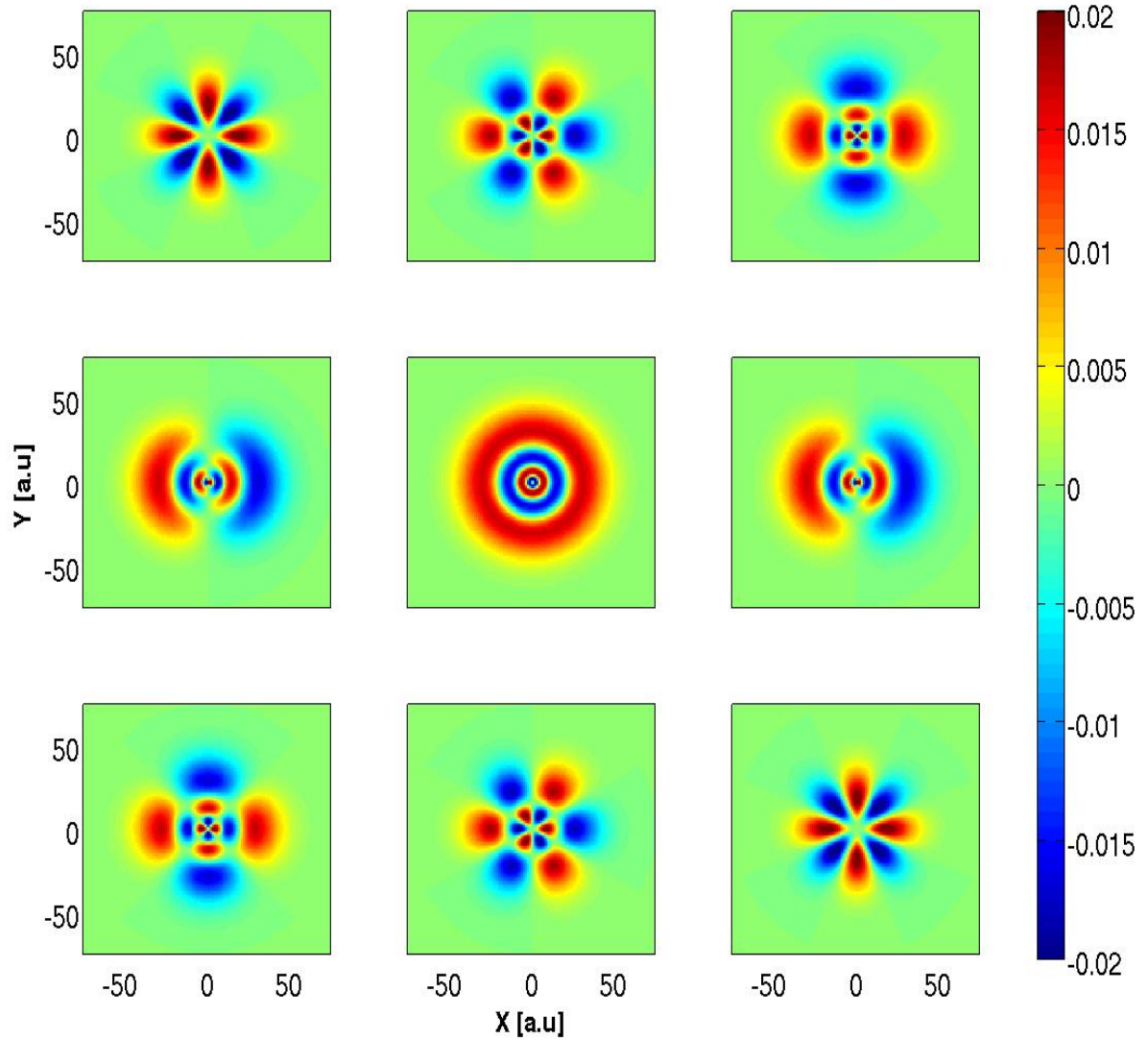


Figure 4.2: The real part of the basis wavefunctions for $n=5$ and $m=-4, \dots, 0, \dots, 4$.

We notice that the real part of the total wavefunction is identical for wavefunctions with the same absolute value of the angular quantum number. This can be explained by the form of the angular solution, which can be rewritten as

$$e^{-im\phi} = \cos(m\phi) - i \sin(m\phi). \quad (4.29)$$

The real part only depends on the cosine and its value is not dependent on the sign of m . Correspondingly the imaginary part will have opposite values for wavefunction with the same $|m|$. From Figure 4.2 we can also identify the angular nodes, and notice that they follow the relation of $|m| = \text{number of angular nodes}$

The rules for nodes are

$$\begin{aligned}
 \text{Total nodes} &= n - 1 \\
 \text{Angular nodes} &= m \\
 \text{Radial nodes} &= n - m - 1
 \end{aligned}
 \tag{4.30}$$

Because of the nodes and the different signs of the wavefunctions for the real and imaginary parts, the correct combinations of the two can form polarized states in a selected direction. From a basis of k states, we can create k new linearly independent combinations of the states. The resulting polarized states are shown in Figure 4.3.

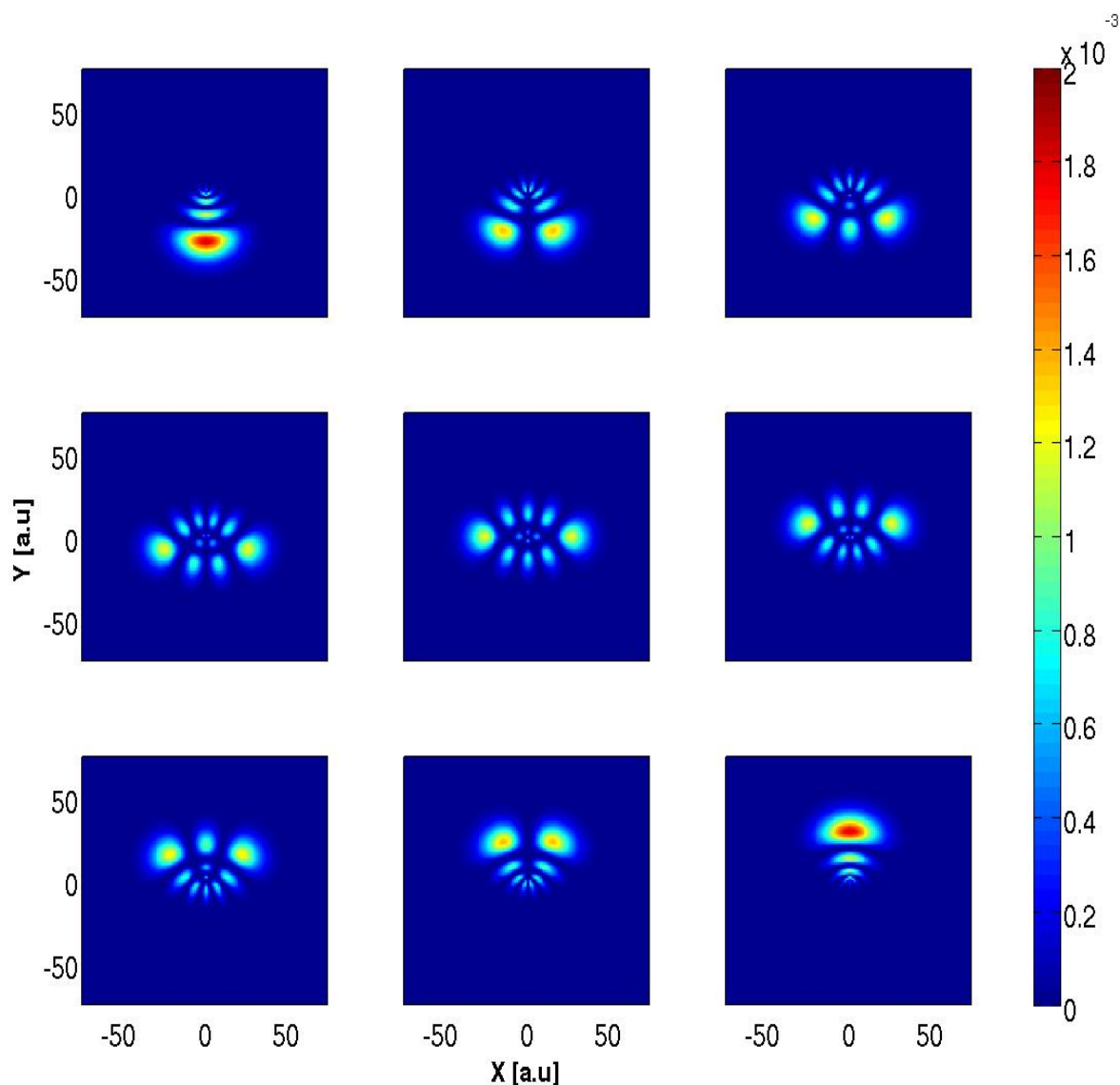


Figure 4.3: This figure shows the polarized states that occur when the $n = 5$ -states are affected by an y-polarized electric field.

The most polarized states are states 1 and 9, so the goal is to optimize population in one of these.

First we calculate the coupling elements. Different from the asymmetrical well, here there are only transitions from state m to $m \pm 1$. The result is that it will be harder to do a successful optimization. The coupling matrix is as shown in Table B.2 in Appendix A. We choose to set our target as the 9th state in Figure 4.3. This state has the linear combination shown in Table 4.1 and a polarization value of $y = 26.9748$.

Table 4.1: The values of the development coefficients $c_1 \dots c_9$ for the polarized state shown in frame 9 in 4.3.

Basis state	Development coefficient value
Ψ_1	0.0625
Ψ_2	$0 + 0.1768i$
Ψ_3	-0.3307
Ψ_4	$0 - 0.4677i$
Ψ_5	0.5229
Ψ_6	$0 + 0.4677i$
Ψ_7	-0.3307
Ψ_8	$0 - 0.1768i$
Ψ_9	0.0625

We will now try to optimize a transition from all the available states to the target state. The matrices are set up similarly like the one in the multi-initial asymmetrical well example, but now we will start in all 9 available basis states. The coupling matrix will thus be a nine times replica of the one in Table B.2 and the energies will be multiplied similarly.

The simulation parameters are as listed in Table 4.2

Table 4.2: The simulation parameters for the optimization from all available initial states to the most polarized state.

Simulation parameter	Value
Basis size	81
Propagation time	5000
Time step	0.05
Initial field	Constant with amplitude 0.05
Max iterations	50
Yield	0.999
Mask	$\sin(\pi \cdot t/T)^2$
Penalty factor	5

The results are unfortunately not very promising. The development of the yield and the total functional are shown in Figure 4.4.

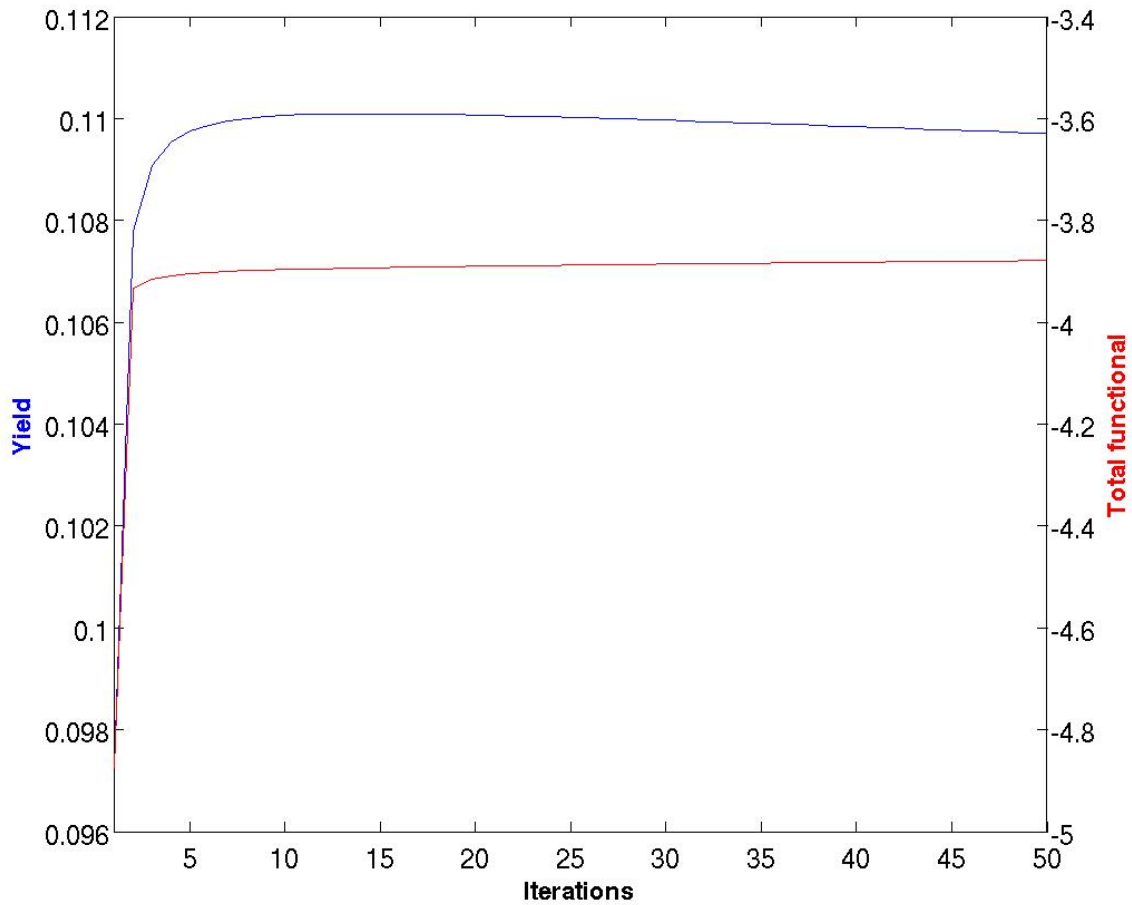


Figure 4.4: The development of the yield in blue and the total functional in red for the 50 step optimization.

We notice that while the functional is still increasing slowly after 50 iterations, implying a successful optimization, the yield already reached its peak after 14 iterations at 0.1101. After 14 iterations the increase in the total functional stems from a reduction in the flux that outweighs the reduction in yield. This is quite revealing as the penalty factor is only set to 5, which should favour a yield maximization rather than a field reduction.

This first observation tied with that the yield limit is almost exactly $1/9$, means that we again reach this seemingly theoretical boundary of maximum $\frac{1}{\text{initial states}}$ yield for multi-initial optimization. It looks like it is impossible to increase the yield beyond this point and any further probing will only lead to less fluence. The yield indicates that one of the 9 starting states should have reached the state after the 50 iterations. In Figure 4.5 the final state for all of the initial states are plotted.

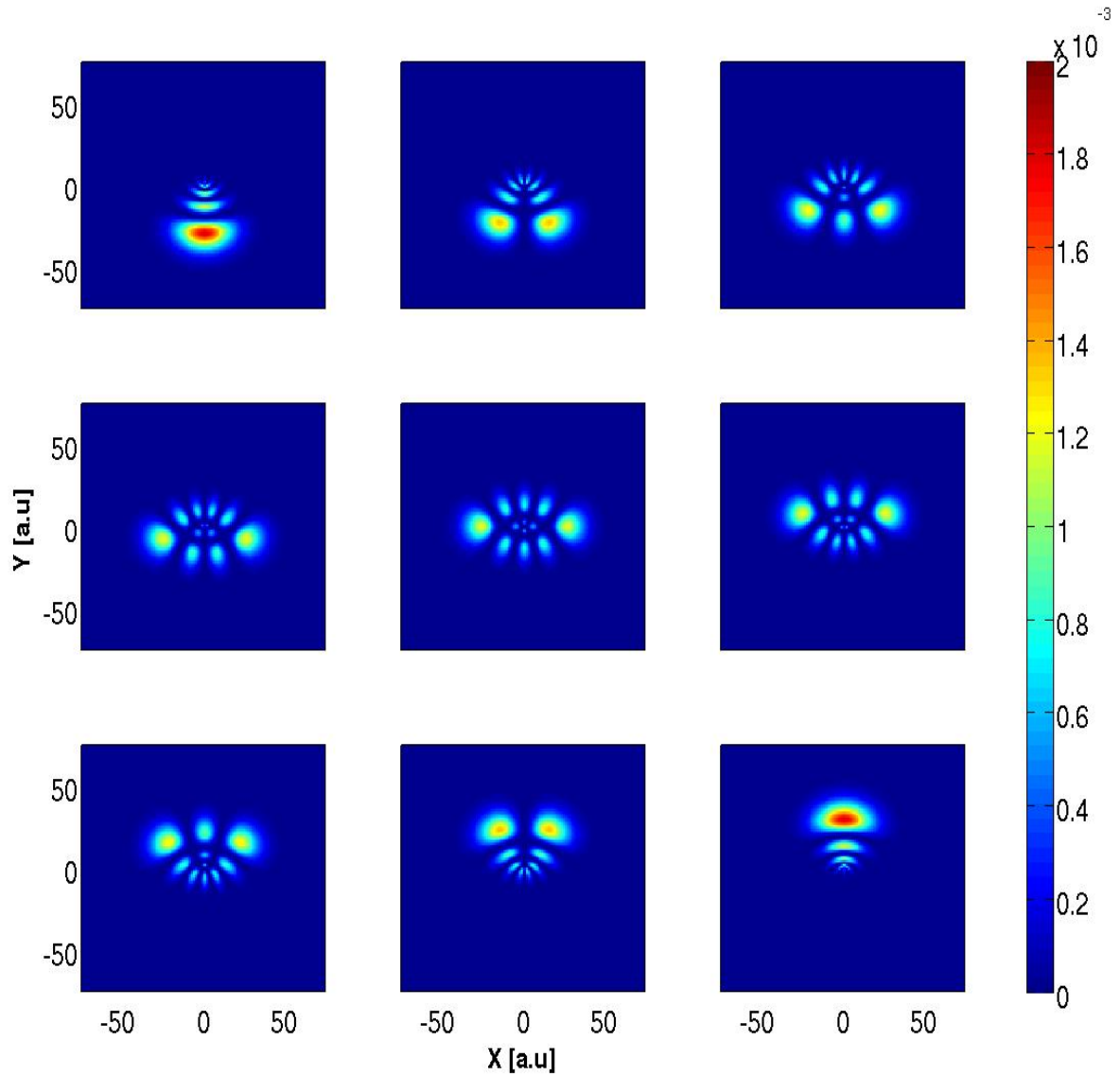


Figure 4.5: The final states for all the initial states in the 2D $n=5$ optimization.

The result of the optimization is that we end in all the available polarized states instead of just in the 9th state. Only the particle that originated from the $\Psi_{m=4}$ state is transferred to the desired polarized state. If we take a closer look at the density distribution for each of the starting states in Figure 4.6 we realize that the result of the optimization for states with the same $|m|$ -value are exact mirrors of each other, while the $m = 0$ state is completely symmetrical.

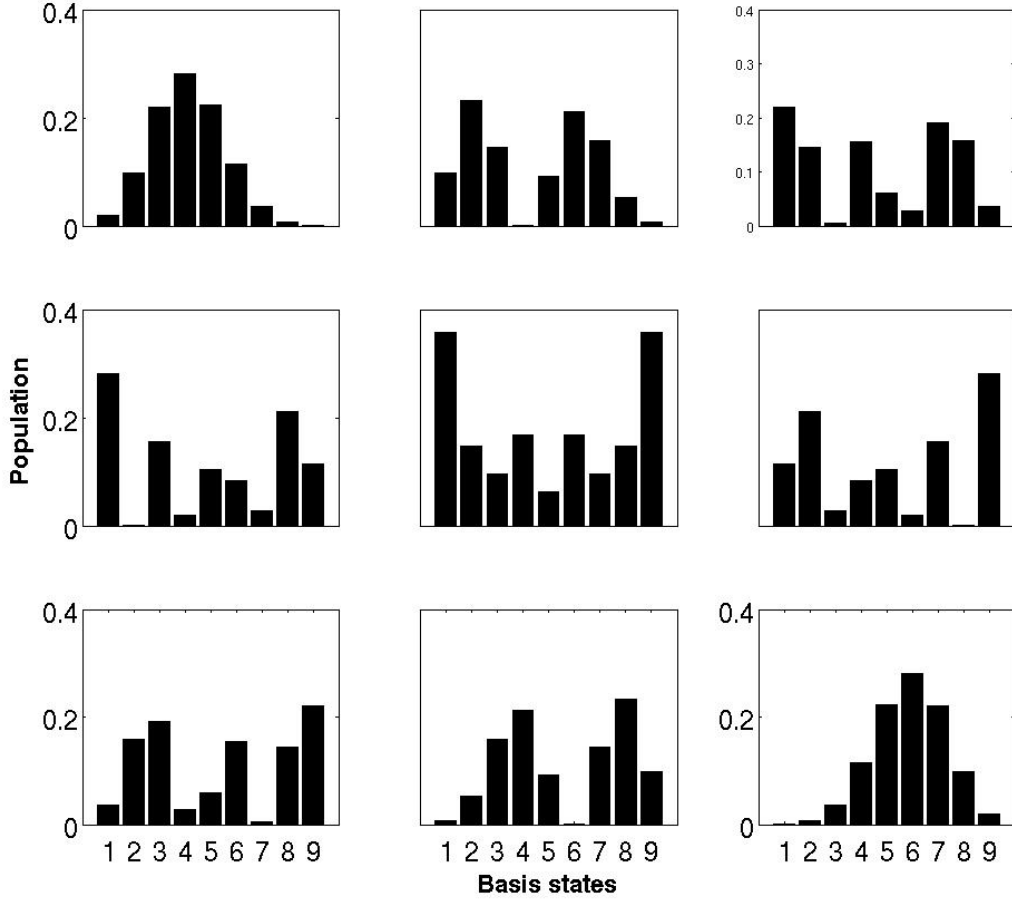


Figure 4.6: The density distribution after the 50 iterations for each of the 9 starting basis states.

To understand this we study the system parameters in Tables B.2 and B.1. Firstly the energies are degenerated, there is no difference between the states and thus it cannot be used to differentiate the effect of the laser pulse on the different states. Secondly the coupling values are also mirrored of each other. The coupling from the $\Psi_{m=-4}$ to $\Psi_{m=-3}$ is equal to the coupling between $\Psi_{m=4}$ and $\Psi_{m=3}$ and this is true for all the couplings. The result is that the field that tries to take an electron starting in $\Psi_{m=4}$ to the linear combination in Table 4.1 will simultaneously take the electron starting in the $\Psi_{m=-4}$ to the direct opposite values leading to the state with opposite polarization.

4.3 Comparison of individual and joint optimization for initial state in $\Psi_{n=5,m=-4}$ and $\Psi_{n=5,m=4}$

By comparing a single optimizations for two states and then look at a combined optimization we will solidify the result we found in the previous Section. By starting in Ψ_1

Table 4.3: The simulation parameters for the optimization for the transitions from $|m| = 4$ to the most polarized state.

Simulation parameter	Value
Basis size	9
Propagation time	200
Time step	0.05
Initial field	Constant with amplitude 0.05
Max iterations	50
Yield	0.999
Mask	$\sin(\pi \cdot t/T)^2$
Penalty factor	5

Table 4.4: The result of the optimization from basis state 1 to the polarized state.

Parameter	Value
Yield	0.9525
Total functional	0.8302
Norm	1.0000

and then in Ψ_9 and using the simulation parameters summarized in Table 4.3 we get the results in Tables 4.4 and 4.5, and as shown in Figures 4.7 and 4.8.

Table 4.5: The result of the optimization from basis state 9 to the polarized state.

Parameter	Value
Yield	0.9971
Total functional	0.9883
Norm	1.0000

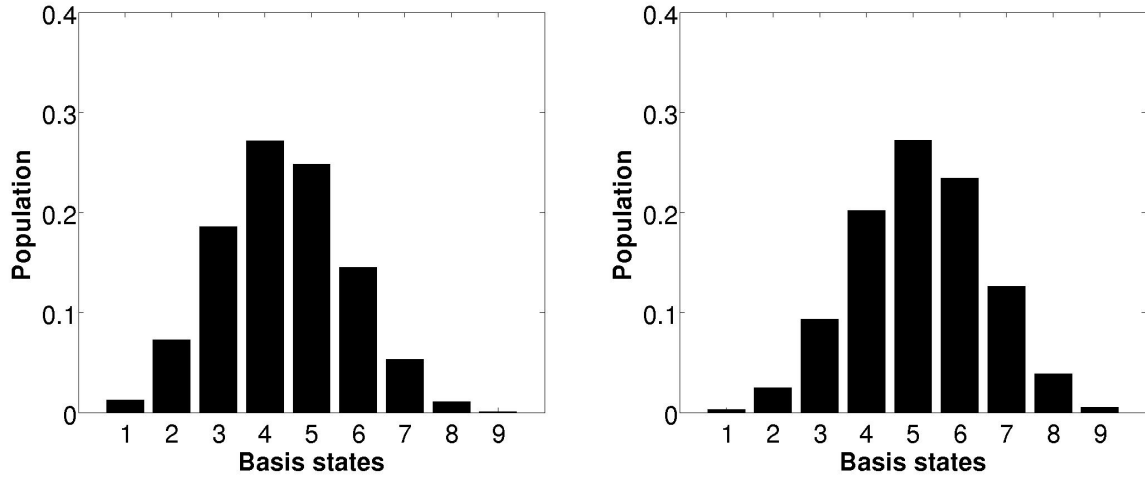


Figure 4.7: The density distribution for the two different initial states after each individual optimization. The distribution for start in basis state 1 and 9, from left to right respectively.

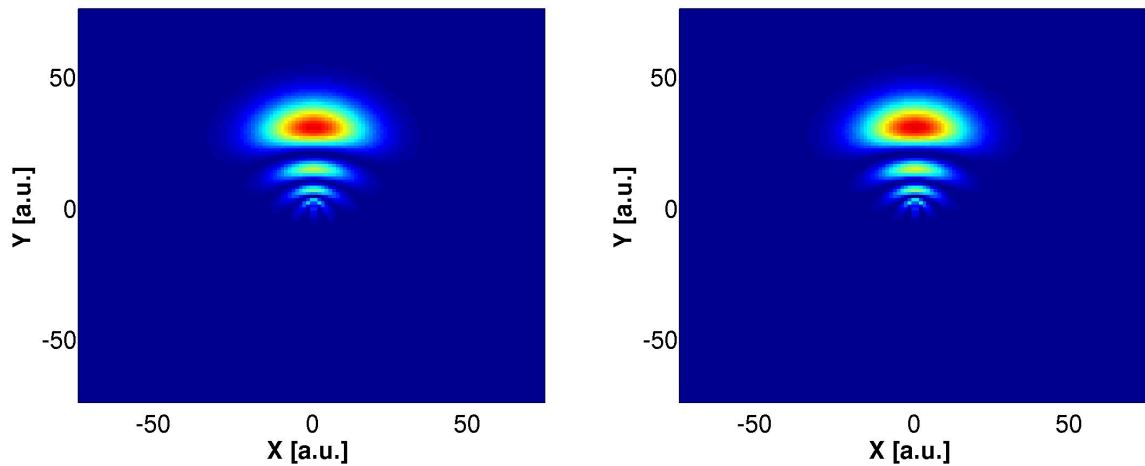


Figure 4.8: The final polarized state for the two different initial states after each individual optimization. The polarized state from start in basis state 1 and 9 from left to right respectively.

We see that both optimizations are successful with high yields and a final states very similar to our desired target. Individually it is possible to optimize transitions from both Ψ_1 and Ψ_9 . However, if we try to do the optimization for both state at the same time with otherwise identical simulation parameters, the result changes as seen in Figures 4.9 and 4.10.

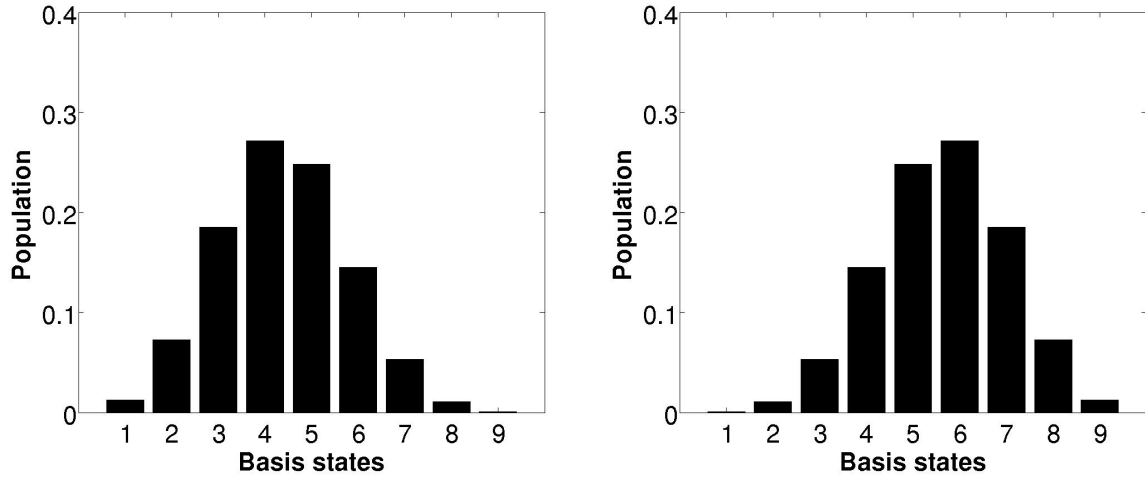


Figure 4.9: The density distribution for the two different initial states after the joint optimization. The distribution for start on basis state 1 and 9, from left to right respectively.

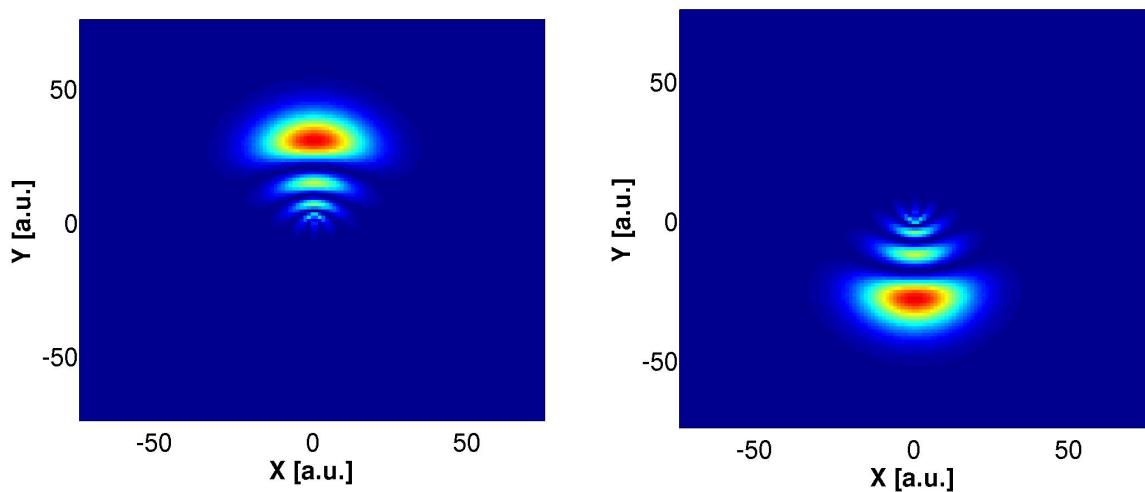


Figure 4.10: The final polarized state for the two different initial states after the joint optimization. The polarized state from start in basis state 1 and 9 is to the left and right respectively.

From the density distribution in Figure 4.9 we see that it is symmetrical for the two states, which results in the two opposite polarizations, shown in Figure 4.10. It is clear that the symmetry of the hydrogen atom is a limiting factor in our goal to optimize multi-initial systems. While it may be possible to optimize a transitions for a any single of the basis states, it is not possible if you start in two states with opposite angular quantum number. The final results are summarized in Table 4.6. In this optimization we normalized each initial state to 1, so the maximum yield for each of the states is 1. This explain why the yield is as high as it is in Table 4.6 which is almost the same yield as the for the single optimization from Ψ_1 to the target state. It is interesting that the optimization optimized this transition instead of the transition from Ψ_9 which yielded a

slightly better result. This may be a result from our initial guess for the field which gets the optimization stuck in this solution.

A special case is that a start in an initial state with $m=0$ will not be successfully transferred to the targeted polarization state even in a single optimization. From the coupling values in Table B.2 we see that every value is mirrored across the $m=0$ state. So any attempt to push the particle from its initial state to a target state would at the same time push it equally to the opposite target state. Thus a polarized state is not possible to achieve from the $m=0$ state in this situation.

Table 4.6: The result of the optimization from basis states 1 and 9 to the polarized state.

Parameter	Value
Yield	0.9526
Total functional	0.8304
Norm	2.0000

4.4 Summary

In this chapter we have found the wavefunctions for the two dimensional hydrogen atom and seen how we can combine them to get polarized states. We have also tried to optimize the population in the the most polarized state in positive y-direction, but is finding some problems.

We still encounters the problem of limitation on the yield due to multiple-initial states, and it does not seem like there is any obvious solution to this problem. However in this chapter we have also seen that the geometry of he hydrogen atom can be an obstacle. Due to degenerated energy-states and coupling values that are mirror of each other, it is impossible to do an optimization on states that starts in opposite initial states.

In a real hydrogen there will be other n -levels available, however the inclusion of these will not improve the result. There will be more allowed transitions, but the coupling values will still be symmetrical across the different levels.

To try to counter this problem we need something to break the symmetry, which will make it possible for the field to distinguish specific transitions. We will take this into account when we continue to the three dimensional hydrogen atom in the next Chapter.

Chapter 5

Three Dimensional Hydrogen in Magnetic Field

We move on from our description of the 2-dimensional hydrogen atom, to the 3-dimensional problem. We will now solve the time-independent Schrödinger equation for the coulomb problem in three dimension which is described in detail in [30].

5.1 The three-dimensional Coulomb problem

As in the 2-dimensional problem, we do a transformation on the coordinates, Cartesian to spherical coordinates. The transformation is

$$\begin{aligned}x &= r \sin \theta \sin \phi, \\y &= r \sin \theta \cos \phi, \\z &= r \cos \theta.\end{aligned}\tag{5.1}$$

The inverse transformations are

$$\begin{aligned}r &= \sqrt{x^2 + y^2 + z^2}, 0 \leq \theta \leq \pi, \\ \phi &= \tan^{-1}\left(\frac{y}{x}\right), 0 \leq \phi \leq 2\pi, \\ \theta &= \tan^{-1}\left(\frac{\sqrt{x^2 + y^2}}{z}\right).\end{aligned}\tag{5.2}$$

Through transformation we get the following Laplace operator,

$$\nabla^2 = \frac{\partial^2}{\partial r^2} + \frac{2}{r} \frac{\partial}{\partial r} + \frac{1}{r^2} \left(\frac{\partial^2}{\partial \theta^2} + \cot \theta \frac{\partial}{\partial \theta} + \frac{1}{\sin^2 \theta} \frac{\partial^2}{\partial \phi^2} \right).\tag{5.3}$$

The last part is identified as the the squared angular momentum operator

$$\hat{L}^2 = - \left(\frac{\partial^2}{\partial \theta^2} + \cot \theta \frac{\partial}{\partial \theta} + \frac{1}{\sin^2 \theta} \frac{\partial^2}{\partial \phi^2} \right). \quad (5.4)$$

The time-independent Schrödinger equation becomes

$$-\frac{1}{2} \left(\frac{\partial^2}{\partial r^2} + \frac{2}{r} \frac{\partial}{\partial r} - \frac{\hat{L}^2}{r^2} \right) \psi(\vec{r}) + V(\vec{r})\psi(\vec{r}) = E\psi(\vec{r}). \quad (5.5)$$

If the potential in equation (5.5) is only dependent on the distance ($V(\vec{r}) = V(r)$), we can separate the variables as in the two dimensional case by stating that $\psi(r, \theta, \phi) = R(r)Y(\theta, \phi)$. We can then solve the two eigenvalue problems, one for the angular part

$$\hat{L}^2 Y(\theta, \phi) = l(l+1)Y(\theta, \phi), \quad (5.6)$$

and one for the radial part,

$$\left[-\frac{1}{2} \left(\frac{\partial^2}{\partial r^2} + \frac{2}{r} \frac{\partial}{\partial r} - \frac{l(l+1)}{r^2} \right) + V(r) \right] R(r) = ER(r). \quad (5.7)$$

5.1.1 Angular Solutions

The angular momentum components are defined as follows

$$\hat{L}_x = z \frac{\partial}{\partial y} - y \frac{\partial}{\partial z}, \hat{L}_y = x \frac{\partial}{\partial z} - z \frac{\partial}{\partial x}, \hat{L}_z = y \frac{\partial}{\partial x} - x \frac{\partial}{\partial y}. \quad (5.8)$$

By transforming them to spherical coordinates and add the squares of hem together we find that

$$\hat{L}^2 = \hat{L}_x^2 + \hat{L}_y^2 + \hat{L}_z^2, \quad (5.9)$$

$$\hat{L}_z = -i \frac{\partial}{\partial \phi}. \quad (5.10)$$

Notice that \hat{L}^2 commutes with all of its components, $[\hat{L}^2, \hat{L}_i] = 0$, $i = x, y, z$, but the components do not commute with each other. This means that we simultaneously can find eigenfunctions to both \hat{L}_z and \hat{L}^2 . We do a new variable separation, $Y(\theta, \phi) = \Theta(\theta)\Phi_m(\phi)$. The eigenvalue equation for \hat{L}_z is

$$\hat{L}_z \Phi(\phi) = m\Phi(\phi) \Rightarrow \Phi_m(\phi) = e^{im\phi}. \quad (5.11)$$

As in the the 2D case the condition $\Phi_m(0) = \Phi_m(2\pi)$ states that m must be an integer or zero. The eigenvalue equation for $\Theta(\theta)$ becomes

$$\left(\frac{\partial^2}{\partial \theta^2} + \cot \theta \frac{\partial}{\partial \theta} + \frac{m^2}{\sin^2 \theta} \right) \theta(\theta) = l(l+1)\Theta(\theta). \quad (5.12)$$

Substituting $\zeta = \cos(\theta)$ we get the following equation

$$\left[(1 - \zeta^2) \frac{\partial^2}{\partial \zeta^2} - 2\zeta \frac{\partial}{\partial \zeta} + l(l+1) - \frac{m^2}{1 - \zeta^2} \right] P_l^m(\zeta) = 0. \quad (5.13)$$

We suppose $P_l(\zeta)$ solves the equation for $m = 0$

$$\left[(1 - \zeta^2) \frac{\partial}{\partial \zeta^2} - 2\zeta \frac{\partial}{\partial \zeta} + l(l+1) \right] P_l(\zeta) = 0 \quad (5.14)$$

Differentiating the above equation $|m|$ times gives

$$\left[(1 - \zeta^2) \frac{\partial^2}{\partial \zeta^2} - 2\zeta \frac{\partial}{\partial \zeta} + l(l+1) - \frac{m^2}{1 - \zeta^2} \right] (1 - \zeta^2)^{\frac{|m|}{2}} \frac{d^{|m|} P_l(\zeta)}{\partial \zeta^{|m|}} = 0, \quad (5.15)$$

From which it follows that

$$P_l^{|m|}(\zeta) = (1 - \zeta^2)^{\frac{|m|}{2}} \frac{\partial^{|m|} P_l(\zeta)}{\partial \zeta^{|m|}} \quad (5.16)$$

are solutions of Equation 5.13 for $m = 0, \pm 1, \pm 2, \dots$ m appears as m^2 in the equation and therefore negative m are included. $P_l(\zeta)$ are the Legendre polynomials, for $l = 0, 1, \dots$, and P_l^m are the associated Legendre polynomials which are known as seen in [30]. The Legendre polynomial $P_l(\zeta)$ is a polynomial of degree l , thus $P_l^m(\zeta)$ is nonzero only when $|m| \leq l$.

5.1.2 Radial solutions

Following [30] we find the radial 3D solution.

$$\left[-\frac{1}{2} \left(\frac{\partial^2}{\partial r^2} + \frac{2}{r} \frac{\partial}{\partial r} - \frac{l(l+1)}{r^2} \right) + V(r) - E \right] R(r) = 0. \quad (5.17)$$

Again we introduce an auxiliary function, $u(r) = rR(r)$ together with

$$\begin{aligned} \rho &= 2\epsilon r \\ E &= -\frac{\epsilon^2}{2}, \end{aligned} \quad (5.18)$$

and rewrite equation (5.17) as

$$\left(\frac{\partial^2}{\partial \rho^2} - \frac{l(l+1)}{r^2} + \frac{1}{\epsilon \rho} - \frac{1}{4} \right) u(\rho) = 0 \quad (5.19)$$

When $\rho \rightarrow \infty$ equation (5.19) reduces to

$$\frac{\partial^2 u(\rho)}{\partial \rho^2} \simeq \frac{1}{4} u(\rho). \quad (5.20)$$

Here the non-divergent solution is $e^{-\frac{\rho}{2}}$. When $\rho \rightarrow 0$, the term $\frac{l(l+1)}{2\rho^2}$ is dominant and we get

$$\frac{\partial^2 u(\rho)}{\partial \rho^2} \simeq \frac{l(l+1)}{\rho^2} u(\rho). \quad (5.21)$$

The non-singular solution is ρ^{l+1} .

Based on these results we try with the product solution

$$u(\rho) = \mathcal{N}_{nl} e^{-\rho/2} \rho^{l+1} h(\rho), \quad (5.22)$$

giving the final equation

$$\rho \frac{\partial^2 h}{\partial \rho^2} + (2l+2-\rho) \frac{\partial h}{\partial \rho} + \left(\frac{1}{\epsilon} - 1 - l \right) h = 0. \quad (5.23)$$

This equation can be identified with the associated Laguerre differential equation,

$$x \frac{\partial^2 h}{\partial x^2} + (\nu + 1 - x) \frac{\partial h}{\partial x} + \lambda h = 0. \quad (5.24)$$

with $\nu = 2l + 1$ and $\lambda = \frac{1}{\epsilon} - 1 - l$. The above equation has solution in terms of the associated Laguerre polynomials, $L_\lambda^{(\nu)}(\rho)$,

$$L_\lambda^{(\nu)}(\rho) = \sum_{i=0}^{\lambda} (-1)^i \frac{(\lambda + \nu)!}{(\lambda - i)! (\nu + i)! i!} \rho^i, \quad (5.25)$$

with $\lambda = \frac{1}{\epsilon} - 1 - l = 0, 1, 2, \dots$. The associated Laguerre polynomials are of order λ . From the solution we obtain the recursion relation for the coefficients in the series above

$$a_{i+1} = \frac{\lambda - i}{(i+1)(\nu + i + 1)} a_i. \quad (5.26)$$

The polynomial solution arises from attempting the infinite power series solution $\sum_{i=0}^{\infty} a_i \rho^i$. The resulting series will not converge for all ρ and should be terminated after a finite number of terms. From the recursion relation we see that this requires $\lambda = 0, 1, 2, \dots$ and we obtain the associated Laguerre polynomials.

Furthermore we define the principal quantum number to be

$$n = \frac{1}{\epsilon}, \quad (5.27)$$

and from the expression for λ it is seen that

$$\begin{aligned} n &= 1, 2, 3, \dots \\ l &\leq n - 1. \end{aligned} \quad (5.28)$$

The bound state energy can be solved for using the definitions $E = -\frac{1}{2}\epsilon^2$, $\lambda = \frac{1}{\epsilon} - 1 - l$ and lastly $n = \frac{1}{\epsilon}$, which gives

$$E_n = -\frac{1}{2n^2}, n = 1, 2, 3, \dots \quad (5.29)$$

In total this gives

$$R_{nl}(\rho) = \mathcal{N}_{nl} e^{-\rho/2} \rho^l L_{n-l-1}^{(2l+1)}(\rho), \quad (5.30)$$

with normalisation constant

$$\mathcal{N}_{nl} = \left(\frac{2}{n}\right)^{3/2} \times \left[\frac{(n-l-1)!}{2n(n+l)!} \right]^{1/2}. \quad (5.31)$$

In total we have not found an expression for the solutions to the 3D Coulomb problem.

5.2 Matrix elements for hydrogen in a magnetic field

The problem we experienced in the 2D case was connected to the symmetry of the potential. The degenerated energies of the atomic states as the symmetric coupling elements made it impossible for a field to optimize selected transitions. In the 3D case we still have a highly symmetric potential and the same problems would naturally occur here as well.

However in the AEGIS project the antihydrogen atoms are stabilized in a strong magnetic field and this leads to a splitting in the energy called the Zeeman effect.

The Hamilton operator for a particle in an electric and magnetic field included the quadratic term is as follows,

$$\hat{H} = H_0 + \mathbf{r} \cdot \mathbf{E}(t) + \frac{\hat{\mathbf{L}}_z \mathbf{B}_z(t)}{2} + \frac{B_z^2}{8}(x^2 + y^2). \quad (5.32)$$

The energy of the unperturbed Hamilton operator to the hydrogen atom is calculated from equation (5.29). We have already found that the eigenvalues from the \hat{L}_z operator is m , so the change to energy from the first magnetic interaction becomes

$$\Delta E = \frac{m}{2}B, (m = -l, -l + 1, \dots, l - 1, l). \quad (5.33)$$

For the last part of the Hamiltonian we need to do calculation over $r^2 \sin^2 \theta$ and for any interaction with the electric field we need to do another calculation over one of the coordinates (x,y,z). These calculations are done by using the work laid out in [48].

$$\begin{aligned} \langle n_2 l_2 | r^k | n_1 l_1 \rangle &= \frac{2^{l_1+l_2+2} b^k (n_2-n_1)^{n_2-l_2-1}}{(n_1+n_2)^{n_2+l_1+k+2}} n_1^{l_2+k+1} n_2^{l_1+k+1} \\ &\left[\frac{(n_1-l_1-1)!(n_2-l_2-1)!}{(n_1+l_1)!(n_2+l_2)!} \right]^{\frac{1}{2}} \sum_{q=0}^{n_1-l_1-1} \sum_{m=0}^{n_2-l_2-1} \frac{(-1)^q 2^{q+m} n_1^m n_2^q}{q!(n_1+n_1)^q (n_1-n_2)^m} \\ &\binom{n_1+l_1}{n_1-l_1-1-q} \binom{n_2+l_2}{2l_2+1+m} \binom{l_1-l_2+k+1+q}{m} (l_1 + l_2 + k + 2 + q)! \end{aligned} \quad (5.34)$$

5.3 Optimization of hydrogen atom polarization in magnetic field

Our goal is to optimize the population in a set target state. While it has not been a success in our previous attempts, this time a magnetic field is introduced and that will skew the energy levels assuring a non-degenerated system.

We start this optimization with a hydrogen atom with the $n = 3$ level available. This gives (from our previous equations) the angular quantum numbers $l = 2, 1, 0$ and magnetic quantum numbers $m = -l, \dots, 0, \dots, l$, in total nine possible states. Undisturbed these basis states will be degenerated as in the 2D case, with the energy $E = -0.0556$. To change this we apply a magnetic field in the z-direction. We see from the new Hamiltonian, equation (5.32), that the Zeeman effect is proportional to the magnitude of the magnetic field. Using equation (5.34) the new energy levels can be calculated. For our system the splitting effect is shown in Figure 5.1.

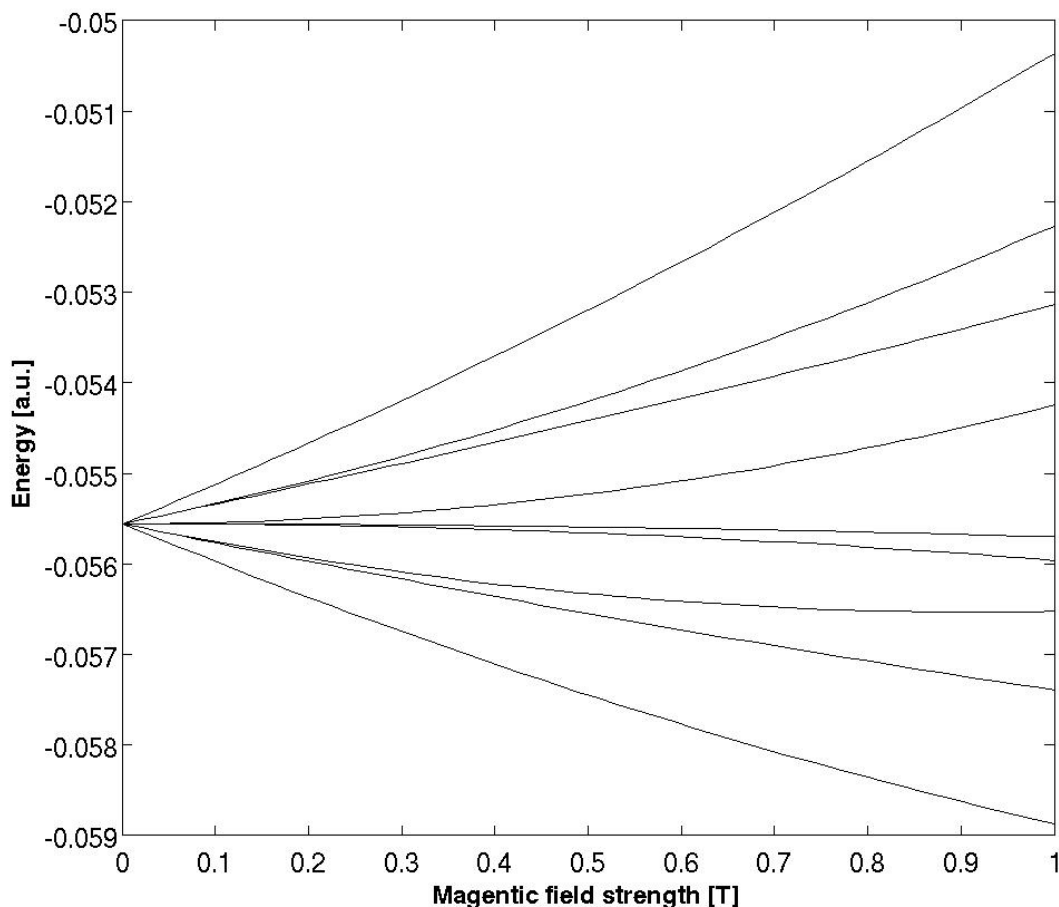


Figure 5.1: The energy splitting effect for increasing magnetic field strength for our $n=3$ level system.

As intended the energy levels are no longer degenerated and we get nine distinct states. It is also promising that the energy differences between the states aren't the same something that was found favourable in [41]. We continue our problem with the states obtained when a constant magnetic field of 1T, is applied. 1T is a strong magnetic field, but it ensures a greater separation between the states and more distinct pulses for each transition. The energies of the new basis states are summarized in Table B.5 in Appendix A. We choose to optimize the Z-polarization, meaning that we need to calculate the coupling values for the new states over Z, or $r \sin \theta$. Again we use equation (5.34) to calculate the coupling elements, shown in Table B.5. From this matrix we obtain the most polarized state in positive Z-direction which we set to be the target state. The Z-value for this state is 9.0 and the development coefficients for the state is shown in Table 5.1.

We notice that the target state only contains the basis states 4, 5 and 6. Combining this with the fact that the only coupling to these states are among themselves, we realise that it is impossible to reach this state from all the initial states. We lay this problem at rest for the moment and do an optimization from all of the available initial states. The

Table 5.1: The values of the development coefficients $c_1 \dots c_9$ for the most polarized state in the positive z-direction.

Basis states	Development coefficient values
Ψ_1	0.0000
Ψ_2	0.0000
Ψ_3	0.0000
Ψ_4	0.6514
Ψ_5	0.7071
Ψ_6	-0.2752
Ψ_7	0.0000
Ψ_8	0.0000
Ψ_9	0.0000

simulation parameters are shown in Table 5.2 while the initial pulse is shown in Figure 5.2.

Table 5.2: The simulation parameters for the 3-level optimisation with common target state.

Simulation parameters	Values
Basis size	81
Propagation time	2000
Time step	0.05
Initial field	$0.01 \cos(0.05t) \cdot \text{mask}$
Max iterations	50
Yield	8.999
Mask	$\text{mask} = \sin(\pi \cdot t/T)^2$
Penalty factor	75

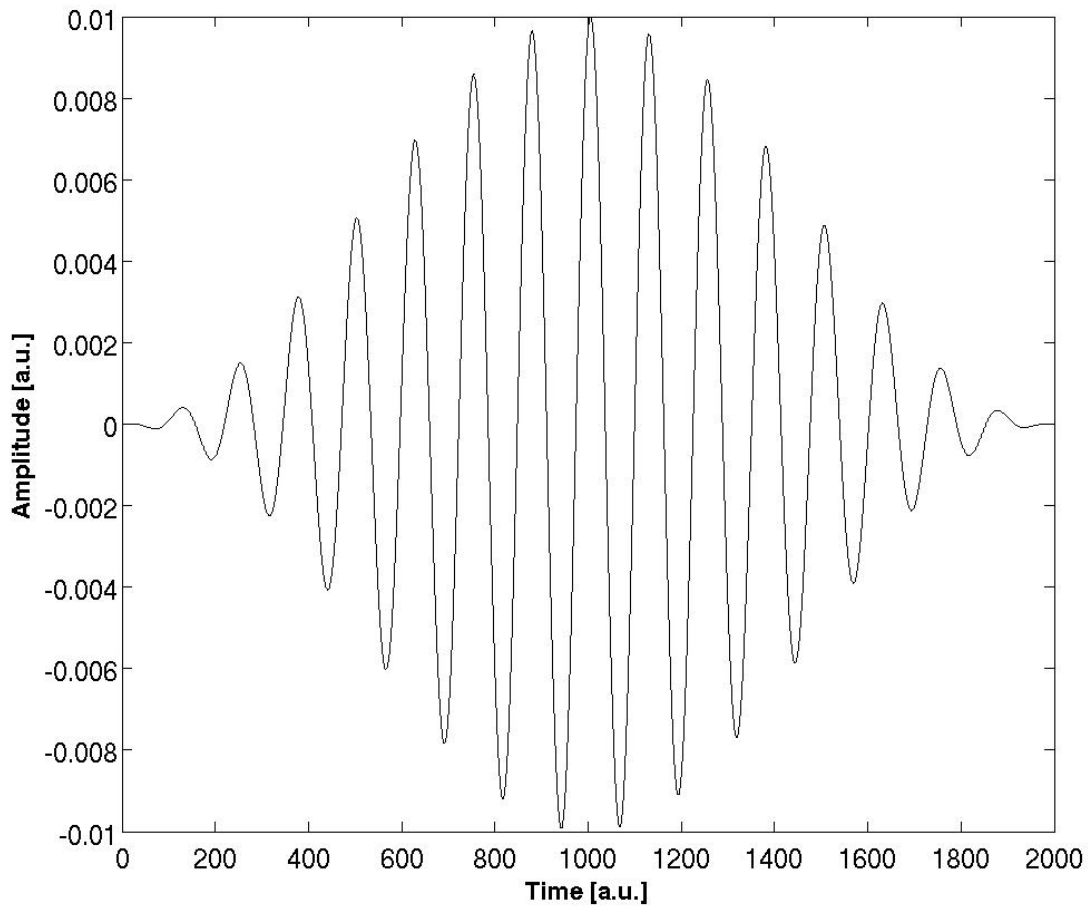


Figure 5.2: The initial testing field.

The results of the optimization are shown in Figure 5.3 and Table 5.3, while the the final optimized field is shown in Figure 5.4.

Table 5.3: The result of the optimization from all the magnetic basis states to the polarized target state.

Parameter	Value
Yield	1.0000
Total functional	-1.5167
Norm	9.0000

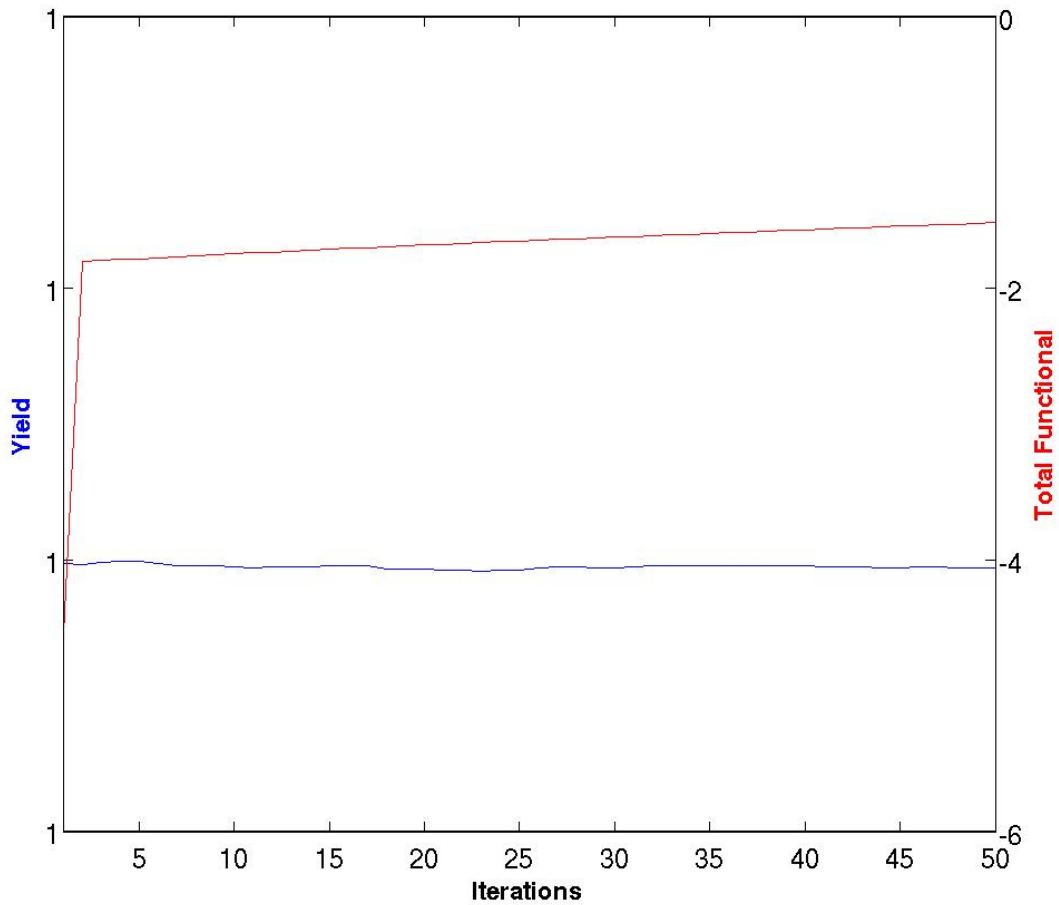


Figure 5.3: The development for the yield (in blue) and the total functional (red) for the two initial optimization.

We notice that the optimization is successful with an increasing functional, however we also note that this is not the merit of the yield. From the start the change in the yield is microscopic and we can conclude that the breaking of the symmetry has not cured all of the problems.

It was expected that the yield would be hampered by the fact that some of the states did not couple to the target state. However the particles that started in the states 4, 5 and 6 should be able to reach the desired polarization. When we look at the field we see that only minor changes have happened and we expect that there has been almost no change in the density distribution from the start.

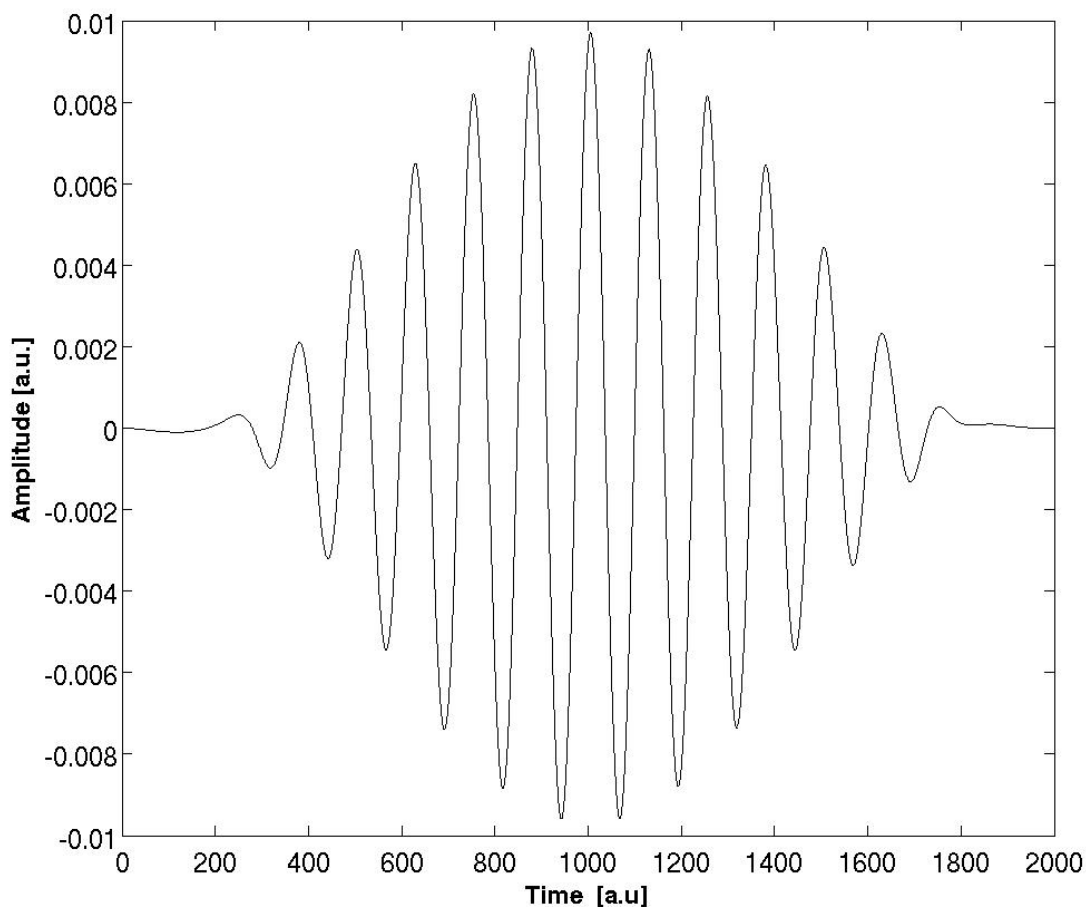


Figure 5.4: The final z-polarized field found in the optimization.

As the symmetry is not longer present there must be another reason for this 1/initial states barrier that blocks our progress. If we go back to the asymmetrical well we remember that we did not achieve the desired outcome that time either, and we suspected that the reason was that the field that optimizes the transition from the initial position to the target position also optimizes the opposite transition. When we want to go from state 4 to the target distribution among states 4,5 and 6, the field will also move the population in initial states 5 and 6 to the opposite distribution. The result is that instead of finding the polarized state the states stay more or less as before.

5.4 Target level optimization

We return to the problem we had with the initial states. As explained most of the initial states had no possibility to reach the target state. However, the particles in these states will not necessarily stay motionless in the field, but will enter new electronic states as the field changes their Hamiltonian as well. We do not know if this state is polarized in

a desired direction. A possible solution is to find additional target states for these initial states.

However if we optimize transition from all possible magnetic basic states in the $n = 3$ level to a possible target state polarized in the correct direction, we encounter a new problem. From the nine available magnetic states we can create nine new polarized states, where three are polarized in the positive z -direction, three in the negative and three are not polarized at all (Table B.6 in appendix A). If we want to do an optimization from each initial state, we have two choices with two different undesired results. Either we choose an individual target state for each initial state, which will lead to a net polarization of zero. Else we give a common target state for some of the initial states which will again result in our earlier problems with a common target state.

The essential problem is that we have too few available target states and our solution is to introduce more of them. In the 2D study inclusion of a second n -level would because of symmetry not improve our results. Here however, we have managed to lose the symmetry and this is also true for higher n -levels as we see in Figure 5.5 and in Tables B.7 and B.8 in Appendix A.

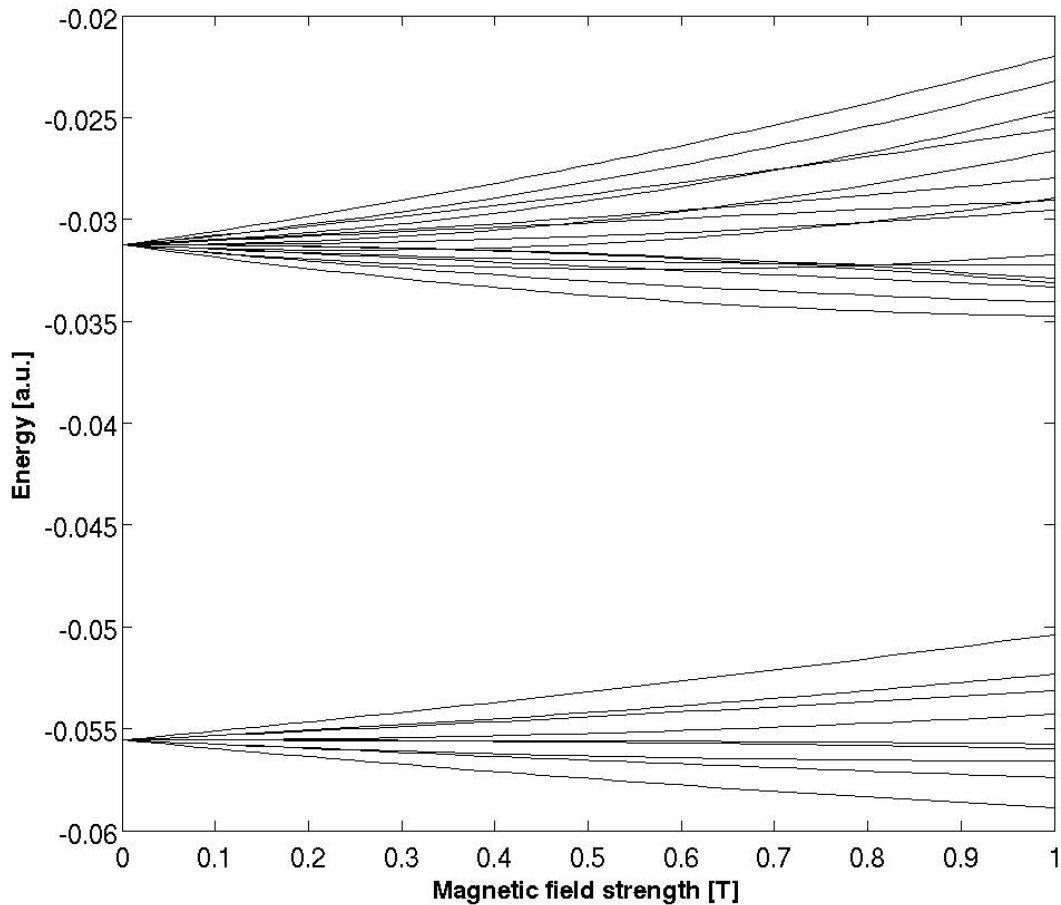


Figure 5.5: The splitting of the energies for the $n = 3$ and $n = 4$ level states.

For the level with principle quantum number $n = 4$ we get the possible angular quantum numbers $l = 3, 2, 1$ and magnetic quantum numbers $m_l = -l, \dots, l$, in total 16 states. From them we get 16 new non-degenerated magnetic states which again can be combined to 16 polarized states of which 10 are polarized in the positive z-direction or not polarized at all as seen in Table B.9. This means that by studying the coupling matrix and the polarized states we can identify an unique target state with positive or zero polarization for each of the nine available initial states. These states are shown in Table 5.4 where the position is marking which initial state it is target for.

Table 5.4: The target states for each of the nine initial states. The first column is the target state for the first initial state etc.

Basis States	Development coefficient								
Ψ_{10}	0.0	0.0	0.0	0.0	0.0	1.0	0.0	0.0	0.0
Ψ_{11}	-0.7071	0.0	0.0	0.0	0.0	0.0	0.0	0.0	0.0
Ψ_{12}	0.0	-0.6102	-0.5052	0.0	0.0	0.0	0.0	0.0	0.0
Ψ_{13}	0.0013	0.0	0.0	0.6632	-0.2453	0.0	0.0	0.0	0.0
Ψ_{14}	0.0007	0.0	0.0	0.6943	-0.1337	-0.0	0.0	0.0	0.0
Ψ_{15}	0.0	0.7071	0.0	0.0	0.0	0.0	0.0	0.0	0.0
Ψ_{16}	0.7071	0.0	0.0	0.0	0.0	0.0	0.0	0.0	0.0
Ψ_{17}	0.0035	0.0	0.0	-0.2453	-0.6632	-0.0	0.0	0.0	0.0
Ψ_{18}	0.0	0.0	0.0	0.0	0.0	0.0	0.5052	0.6102	0.0
Ψ_{19}	0.0	0.3572	-0.8630	0.0	0.0	0.0	0.0	0.0	0.0
Ψ_{20}	0.0	0.0	0.0	0.0	0.0	0.0	0.0	0.7071	0.
Ψ_{21}	-0.0036	0.0	0.0	0.1337	0.6943	0.0	0.0	0.0	0.0
Ψ_{22}	0.0	0.0	0.0	0.0	0.0	0.0	0.0	0.0	-0.7071
Ψ_{23}	0.0	0.0	0.0	0.0	0.0	0.0	0.8630	-0.3572	0.0
Ψ_{24}	0.0	0.0	0.0	0.0	0.0	0.0	0.0	0.0	0.7071
Ψ_{25}	0.0	0.0	0.0	0.0	0.0	0.0	0.0	0.0	0.0

We will now do the optimization from the nine basis states in the magnetic field to the target states. The simulation parameters are summarized in Table 5.5.

Table 5.5: The simulation parameters for the 3-level optimization with common target state.

Simulation parameters	Values
Basis size	25
Propagation time	2000
Time step	0.05
Initial field	$0.01 \cos(0.05t) \cdot \text{mask}$
Max iterations	50
Mask	$\sin(\pi \cdot t/T)^2$
Yield	8.999
Penalty factor	75

The results of the optimization are found in Table 5.6 and Figure 5.6.

Table 5.6: The result of the optimization from the 9 initial states to the 9 individual target states.

Parameter	Value
Yield	1.7638
Total functional	1.6791
Norm	9.0000

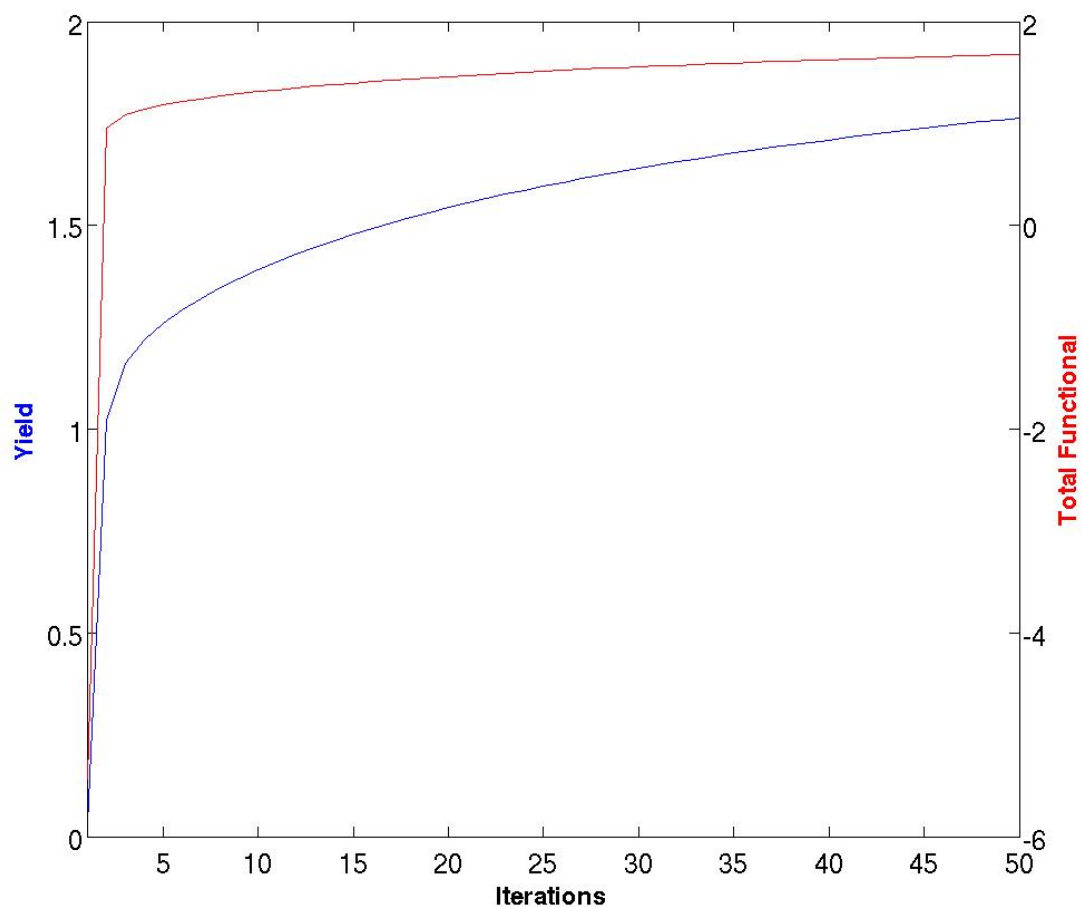


Figure 5.6: The development for the yield (in blue) and the total functional (red) for the multi initial optimization with individual target states.

We see from the development that we finally has broken the 1/initial states yield limit. While a yield of 1.7638 out possible 9 is not a great outcome, it indicates that we can reach higher yield than previously experienced. The convergence of the yield and the functional is positive, and this with minimal shaping of the pulse. The field after 50 iterations is plotted in Figure 5.7.

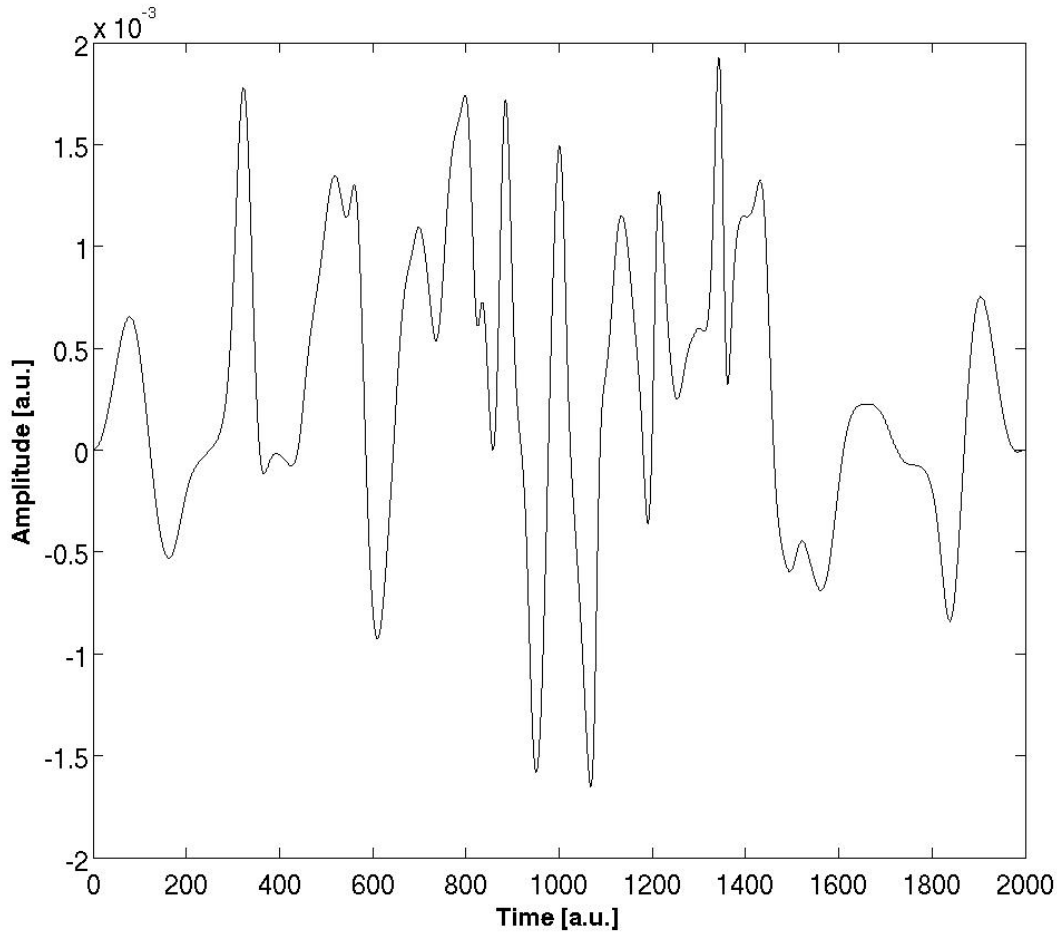


Figure 5.7: The final optimized z-polarized field for the optimization from all the nine initial states in level 3 to each individual target state in level 4.

In this optimization, the field has changed considerably from the initial pulse. In the optimization in Section 4.1 the system mechanics restricted the pulse to do effective optimization and thus there were small changes between the initial and final pulse. Here however, when we introduced 9 initial states and individual target states the field changed considerably. In this optimization we only put on a penalty factor and a mask to restrict the field. I am positive that with more experimentation with filters, more iterations and longer pulse duration, a higher yield could be achieved.

A key factor of this optimization is of course that we have slightly altered our goal. From trying to populate a set target state from all possible initial state, we have moved more over to try to optimize the polarization of the hydrogen atoms. This means that all the hydrogen atoms will not have the same polarization, but our previous results shows that this would not be possible in any case. In this new case we can at least be more certain that the hydrogen atoms will have a polarization in our desired direction. This revelation means that it might be more fruitful to change the operator we want to maximize. In this work I've used an algorithm that optimized the expectation value of the projector

operator $\hat{O} = |\Psi_t\rangle\langle\Psi_t|$, but with our new realisations it might be better to optimize the position operator $\hat{O} = \hat{Z}$. This will probably ensure that most of the initial states reaches different states polarized in the right direction, as we have tried to do here.

One advantage I can see from our approach to go the projection operator path, is a higher control on the transitions we wants to happen. I do believe that with this approach we can put on weight factors on the different initial states to ensure that some are more likely to happen. While the position operator will prefer the transitions to the most polarized state and neglect the less polarized state, we can with the projection operator scale the value of these less populated target states. This means that the J_1 functional will be maximized if this transition is most successful.

5.5 Summary

In this chapter we have shown that by including higher unpopulated n-levels we can design target states for each of the possible states. This is possible because the applied magnetic field breaks the inherit symmetry of the hydrogen atom. By designing individual target states we bypasses the problem we previously experienced with yield restriction. This leads to a larger amount of hydrogen atoms polarized in the correct direction if not in the most polarized state. This should also be possible for higher energy levels, but will demand more work and computational power.

Chapter 6

Conclusion and Outlook

The background for this master thesis was the AEGIS project and the desire to improve the data collection by increasing the amount of antihydrogen that reaches the detector through quantum control and laser manipulation. In this work we have encountered and addressed some of the issues that will be effecting this endeavour, though in much smaller scale.

The main issue of the optimization is the unknown initial conditions. We only know that the antihydrogen atoms will be created in highly excited states with the principle quantum number between $n = 30$ and $n = 40$. This leaves a huge amount of possible initial states which all must be optimized to a desired target state. We learned from our 1D well in Chapter 3 that a single transition optimization is highly achievable, but when we introduce an additional initial state the yield was restricted to half of what possible. This happens even though both initial states could successfully be transferred to the target state on their own. We also found that using a pulse train with pulses from each individual transition did not help and indicated that while a pulse that optimized the transition from an initial state to the target state, also optimizes the opposite transition. This makes the whole concept with identical target states very difficult to accomplish.

In Chapter 4 we studied the 2D hydrogen atom and experienced a second problem. Due to the high symmetry of the hydrogen atom we found that all the optimization parameters were symmetrical or identical. This meant that if two initial states had the opposite angular quantum number, they would end up in opposite polarized state of each other meaning that to try to optimize a polarization of all the available states would be futile. Inclusion of higher levels to find polarized states there was not helpful as the symmetry still was intact. This problem would also have carried on to the similarly symmetrical 3D atom.

In the AEGIS project the antihydrogen atoms are stabilized by a strong magnetic field, and this is of crucial importance as it also affects the energy levels and coupling of the antihydrogen states. We took advantage of this in our 3D hydrogen model in Chapter 5, where we optimized multiple initial states without ending in opposite polarized states. To counter the problem of multiple initial states and common target states we introduced a higher level of available target states, which we could couple an individual initial state

to. This lead to a higher yield than our before mentioned $1/\text{initial states-limit}$.

While the scope of this thesis has been on a much smaller scale and with a hydrogen model instead of antihydrogen, I think it can say something about the possibilities for this project. While we cannot be certain in what states the antihydrogen atoms will be in when they are created, we can make quite good assumptions in where they will not be. In the project description it says that the antihydrogen atoms will be in states between $n = 30$ and $n = 40$. This means that we can create target states for levels higher than this and try to design paths for each of the available target initial states. The next step from this master thesis would be to try to find a unique target state for all the available initial states and do an optimization that get as high yield as possible as well as adjusting the field to be experimentally feasible.

There are some problematic aspect with this of course. The huge amount of designed transitions will demand a very complicated field; maybe too complicated to be able to construct. It may also be that the sheer number of transitions will be impossible to control and the yield will not be as high as desired and it will demand a lot of computer power to calculate the field.

The most important thing is however that we increase the amount of hydrogen or anti hydrogen atoms polarized in the correct direction. Even though we do not achieve a 100% projection, more anti hydrogen atoms will be accelerated towards the detector. This was also true for the 2-dimensional case. While the initial states ends up in direct opposite polarized states and the average polarization is still 0 after the optimization, half of the states are polarized in the correct direction and will be accelerated towards the detector.

In addition to this approach, new angles to address the problem might be applied in future. I have already mentioned that changing the operator to a position operator might be an easier way to achieve the desired polarized states.

Hopefully one of these approaches will one day give a pulse that yields the desired polarization and is experimentally valid. Then it might be applied to the AEGIS project and contribute to get a final answer to one of the mysteries that surrounds antimatter.

Appendix A

Atomic Units

The atomic unit system is often used in calculations on atomic length scales, and this system of units is given in Table A.1 [49].

This system of units is obtained by setting the quantities m_e , e , \hbar and a_0 equal to unity. Quantities that are given in atomic units are abbreviated by the symbol *a.u.*

Table A.1: Table of the atomic unit system and how the quantities are related to the SI system of units

Physical Unit	Unit	Physical origin	Value in SI units
Mass	m	Electron mass	9.10938×10^{-31} kg
Charge	e	Absolute value of the electron charge	1.60218×10^{-19} C
Angular Momentum	\hbar	The reduced Planck's constant	1.05457×10^{-34} Js ⁻¹
Length	a_0	Bohr radius for atomic hydrogen (with infinite nuclear mass)	5.29177×10^{-11} m
Velocity	$v_0 = \alpha c$	Magnitude of electron velocity in first Bohr orbit	2.18769×10^6 ms ⁻¹
Momentum	$p_0 = mv_0$	Magnitude of electron momentum in the first Bohr orbit	1.99285×10^{-24} kg m s ⁻¹
Time	$\frac{a_0}{v_0}$	Time required for electron in first Bohr orbit to travel one Bohr radius	2.41888×10^{-17} s
Frequency	$\frac{v_0}{2\pi a_0}$	Angular frequency of electron in first Bohr orbit divided by 2π	6.57969×10^{15} s ⁻¹

Energy	$\frac{e^2}{4\pi\epsilon_0 a_0}$	Twice the ionization potential of atomic hydrogen (with infinite nuclear mass)	$4.35974 \times 10^{-18} \text{ J}$
Electric field strength	$\frac{e}{(4\pi\epsilon_0) a_0^2}$	Strength of the Coulomb field experienced by an electron in the first Bohr orbit of atomic hydrogen (with infinite nuclear mass)	$5.14221 \times 10^{11} \text{ Vm}^{-1}$

Appendix B

Simulation Matrices

B.1 Two dimensional hydrogen optimization

Table B.1: The principal(n) and angular(m) quantum numbers for the 9 basis states as well as their Energy.

Basis state	n	m	E
Ψ_1	5	-4	-0.0247
Ψ_2	5	-3	-0.0247
Ψ_3	5	-2	-0.0247
Ψ_4	5	-1	-0.0247
Ψ_5	5	0	-0.0247
Ψ_6	5	1	-0.0247
Ψ_7	5	2	-0.0247
Ψ_8	5	3	-0.0247
Ψ_9	5	4	-0.0247

Table B.2: The coupling values between the nine n=5 basis states.

Ψ_i	Ψ_j	Coupling value
1	2	-9.5459
2	3	-12.6280
3	4	-14.3187
4	5	-15.0931
5	6	-15.0931
6	7	-14.3187
7	8	-12.6280
8	9	-9.5459

Table B.3: The sorted polarization values for the 9 polarized states from the n=5 2D basis.

The polarization values
-27.0242
-20.2744
-13.5246
-6.7746
-0.0247
6.7252
13.4752
20.2251
26.9748

B.2 Three dimensional hydrogen optimization

B.2.1 3-level matrices

Table B.4: The energies to the n=3 states separated by the magnetic field.

Basis state	Energy
Ψ_1	-0.0589
Ψ_2	-0.0576
Ψ_3	-0.0565
Ψ_4	-0.0560
Ψ_5	-0.0557
Ψ_6	-0.0542
Ψ_7	-0.0531
Ψ_8	-0.0523
Ψ_9	-0.0504

Table B.5: The coupling matrix for the n=3 states set ut by the magnetic field.

Ψ_i	Ψ_j	Coupling value
2	3	4.5000
4	5	8.2905
4	6	4.7093e-14
5	6	-3.5025
7	8	-4.5000

Table B.6: The sorted polarization values for the 9 polarized states from the n=3 magnetic basis

The polarization values
-9.0000
-4.5000
-4.5000
0
0
0.0000
4.5000
4.5000
9.0000

B.2.2 3- and 4-level matrices

Table B.7: The energies to the n=4 states splitted by the magnetic field.

Basis state	Energy
Ψ_{10}	-0.0347
Ψ_{11}	-0.0341
Ψ_{12}	-0.0333
Ψ_{13}	-0.0331
Ψ_{14}	-0.0329
Ψ_{15}	-0.0322
Ψ_{16}	-0.0317
Ψ_{17}	-0.0296
Ψ_{18}	-0.0291
Ψ_{19}	-0.0290
Ψ_{20}	-0.0280
Ψ_{21}	-0.0267
Ψ_{22}	-0.0255
Ψ_{23}	-0.0247
Ψ_{24}	-0.0232
Ψ_{25}	-0.0220

Table B.8: The coupling matrix for the n=3 and n=4 states.

Ψ_i	Ψ_j	Coupling value
1	11	-3.7123
2	3	4.6163
2	12	4.5915
2	15	7.6543e-15
2	19	-1.0717
3	12	-9.6441e-15

3	15	3.4370
3	19	1.4657e-15
4	5	8.6094
4	6	1.6770e-16
4	13	-4.5086
4	14	7.8847e-14
4	17	-1.7735
4	21	6.4975e-16
5	6	3.4313
5	13	7.1161e-14
5	14	4.1868
5	17	3.4076e-15
5	21	0.9715
6	13	-0.2843
6	14	1.3478e-15
6	17	3.5806
6	21	2.1988e-15
7	8	4.6163
7	18	4.5915
7	20	1.7241e-14
7	23	-1.0717
8	18	-1.2288e-14
8	20	3.4370
8	23	8.2916e-15
9	22	-3.7123
11	16	6.0967
12	15	10.3475
12	19	7.2068e-15
13	14	-16.7950
13	17	7.0502e-14
13	21	1.2149
14	17	5.0636
14	21	-6.6979e-15
15	19	6.1265
17	21	-6.7571
18	20	10.3475
18	23	1.0611e-14
20	23	6.1265
22	24	6.0967

Table B.9: The sorted polarization values for the 9 polarized states from the n=4 magnetic basis.

The polarization values
-18.0000
-12.0000
-12.0000
-6.0000
-6.0000
-6.0000
-0.0000
0.0000
0.0000
0.0000
6.0000
6.0000
6.0000
12.0000
12.0000
18.0000

Appendix C

Programs

During this thesis a number of programs have been developed in MATLAB. These include a program to calculate the energies and coupling matrix as well as the target state for all the systems. There was also developed a converter program and a visualization program.

C.1 1D asymmetrical well

A program was created to find energies and the wavefunction of the 1D asymmetrical well. This was done using hermite polynomials. The program also calculated the coupling matrix for the basis states and plotted the selected n lowest states in potential s well as one plotting the resulting states of the optimization.

C.2 2D hydrogen atom

A routine was made to find the basis functions of the 2D hydrogen atom, involving Laguerre polynomials. It also calculated the coupling matrix and plotted the radial distributions and the polarized forms of the basis functions. A corresponding routine visualised the resulting polarized forms from the optimization.

C.3 3D hydrogen atom in magnetic field

A Fortran routine calculated the matrix elements for the basis functions. A MATLAB program was made to visualise the effect of the magnetic field, as well as finding the polarized states of the new basis set up by the magnetic field.

C.4 Visualisation program

A program was made to obtain the results from the multi-initial optimizations and visualize the key result such as yield, functional, density distribution and optimized fields.

C.5 Converter

Due to the task of doing multi-initial optimization a routine was made to duplicate all the necessary matrices for all the cases and convert them to be read by the Fortran optimization program.

Bibliography

- [1] T. A. collaboration, “Proposal for the aegis experiment at the cern antiproton decelerator (antimatter experiment: Gravity, interferometry, spectroscopy)”, Available at <http://aegis.web.cern.ch/aegis/Proposal/Proposition.pdf> (2007).
- [2] Wikipedia, “Richard feynman — wikipedia, the free encyclopedia”, [Online; accessed 1-June-2014] (2014).
- [3] R. Feynman, “There is plenty of room at the bottom”, Caltech Engineering and Science **23** (1960), transcript of speech, Available at <http://calteches.library.caltech.edu/47/3/ES.23.5.1960.0.pdf>.
- [4] N. Taniguchi, “On the basic concept of 'nanotechnology'”, (1974).
- [5] C. O. T. E. COMMUNITIES, “Code of conduct for responsible nanosciences and nanotechnologies research”, (2008).
- [6] M. Ardenne, “Das elektronen-rastermikroskop”, Zeitschrift für Physik **109**, 553–572 (1938).
- [7] A. V. Crewe, J. Wall, and J. Langmore, “Visibility of single atoms”, Science **168**.
- [8] G. Binnig and H. Rohrer, “Scanning tunneling microscopy”, Surface Science **126**, 236 – 244 (1983).
- [9] G. Binnig, C. F. Quate, and C. Gerber, “Atomic force microscope”, Physical Review Letter **56**, 930–933 (1986).
- [10] D. M. Eigler and E. K. Schweizer, “Positioning single atoms with a scanning tunnelling microscope”, Nature **344**, 524 (1990), copyright - Copyright Macmillan Journals Ltd. Apr 05, 1990; Last updated - 2012-11-14; CODEN - NATUAS.
- [11] E. Schrödinger, “An undulatory theory of the mechanics of atoms and molecules”, Physical Review **28**, 1049–1070 (1926).
- [12] Wikipedia, “Albert einstein — wikipedia, the free encyclopedia”, [Online; accessed 1-June-2014] (2014).
- [13] Wikipedia, “Max planck — wikipedia, the free encyclopedia”, [Online; accessed 1-June-2014] (2014).
- [14] A. Einstein, “Über einen die Erzeugung und Verwandlung des Lichtes betreffenden heuristischen Gesichtspunkt”, Annalen der Physik **322**, 132–148 (1905).

- [15] M. Planck, “Ueber das Gesetz der Energieverteilung im Normalspectrum”, *Annalen der Physik* **309**, 553–563 (1901).
- [16] W. Heisenberg, “Über den anschaulichen inhalt der quantentheoretischen kinematik und mechanik”, *Zeitschrift für Physik* **43**, 172–198 (1927).
- [17] Wikipedia, “Paul dirac — wikipedia, the free encyclopedia”, [Online; accessed 1-June-2014] (2014).
- [18] Wikipedia, “Erwin schrodinger — wikipedia, the free encyclopedia”, [Online; accessed 1-June-2014] (2014).
- [19] Wikipedia, “Werner heisenberg — wikipedia, the free encyclopedia”, [Online; accessed 1-June-2014] (2014).
- [20] P. A. M. Dirac, “The quantum theory of the electron”, *Proceedings of the Royal Society of London. Series A* **117**, 610–624 (1928).
- [21] C. D. Anderson, “The apparent existence of easily deflectable positives”, *Science* **76**, 238–239 (1932).
- [22] O. Chamberlain, E. Segrè, C. Wiegand, and T. Ypsilantis, “Observation of antiprotons”, *Physical Review* **100**, 947–950 (1955).
- [23] B. Cork, G. R. Lambertson, O. Piccioni, and W. A. Wenzel, “Antineutrons produced from antiprotons in charge-exchange collisions”, *Physical Review* **104**, 1193–1197 (1956).
- [24] T. Massam, T. Muller, B. Righini, M. Schneegans, and A. Zichichi, “Experimental observation of antideuteron production”, *Il Nuovo Cimento A* **63**, 10–14 (1965).
- [25] G. Baur, G. Boero, A. Brauksiepe, A. Buzzo, W. Eyrich, R. Geyer, D. Grzonka, J. Hauffe, K. Kilian, M. LoVetere, M. Macri, M. Moosburger, R. Nellen, W. Oelert, S. Passaggio, A. Pozzo, K. Röhrich, K. Sachs, G. Schepers, T. Sefzick, R. Simon, R. Stratmann, F. Stinzinger, and M. Wolke, “Production of antihydrogen”, *Physics Letters B* **368**, 251 – 258 (1996).
- [26] “Antihydrogen held captive”, *Nature* **474**, 130 (2011), copyright - Copyright Nature Publishing Group Jun 9, 2011; Last updated - 2012-11-14; CODEN - NATUAS.
- [27] L. Canetti, M. Drewes, and M. Shaposhnikov, “Matter and antimatter in the universe”, *New Journal of Physics* **14**(9), 095012 (2012).
- [28] D. Hajdukovic, “Is dark matter an illusion created by the gravitational polarization of the quantum vacuum?”, *Astrophysics and Space Science* **334**, 215–218 (2011).
- [29] Benoit-Lévy, A. and Chardin, G., “Introducing the dirac-milne universe”, *A&A* **537**, A78 (2012).
- [30] P. C. Hemmer, *Kvantemekanikk*, Tapir Akademiske Forlag, (2005).
- [31] A. Einstein, “Zur Quantentheorie der Strahlung”, *Physikalische Zeitschrift* **18**, 121–128 (1917).

- [32] T. H. Maiman, “Stimulated Optical Radiation in Ruby”, *Nature* **187**, 493–494 (1960).
- [33] C. Daniel, J. Full, L. González, C. Lupulescu, J. Manz, A. Merli, Vajda, and L. Wöste, “Deciphering the reaction dynamics underlying optimal control laser fields”, *Science* **299**, 536–539 (2003).
- [34] A. Assion, T. Baumert, M. Bergt, T. Brixner, B. Kiefer, V. Seyfried, M. Strehle, and G. Gerber, “Control of chemical reactions by feedback-optimized phase-shaped femtosecond laser pulses”, *Science* **282**, 919–922 (1998).
- [35] “Quantum optimal control theory: Filter techniques, time-dependent targets, and time-dependent density-functional theory”, Ph.D. thesis.
- [36] H. J. Sussmann and J. C. Willems, “300 years of optimal control: from the brachystochrone to the maximum principle”, *Control Systems, IEEE* **17**(3), 32–44 (1997).
- [37] D. G. Luenberger, *Introduction to dynamic systems*, John Wiley & sons, (1979).
- [38] A. D. Lewis, “The maximum principle of pontryagin in control and in optimal control”, Handouts for the course taught at the Universitat Politècnica de Catalunya (2006).
- [39] L. N. Trefethen and D. Bau III, *Numerical linear algebra*, volume 50, Siam, (1997).
- [40] V. Ramakrishna, M. V. Salapaka, M. Dahleh, H. Rabitz, and A. Peirce, “Controllability of molecular systems”, *Phys. Rev. A* **51**, 960–966 (1995).
- [41] S. Schirmer, H. Fu, and A. Solomon, “Complete controllability of quantum systems”, *Physical Review A* **63**(6), 063410 (2001).
- [42] W. Zhu and H. Rabitz, “A rapid monotonically convergent iteration algorithm for quantum optimal control over the expectation value of a positive definite operator”, *The Journal of Chemical Physics* **109**(2) (1998).
- [43] V. Krotov, “Global methods in optimal control theory”, in *Advances in Nonlinear Dynamics and Control: A Report from Russia*, edited by A. Kurzhanski, volume 17 of *Progress in Systems and Control Theory*, 74–121, Birkhauser Boston, (1993).
- [44] W. Zhu, J. Botina, and H. Rabitz, “Rapidly convergent iteration methods for quantum optimal control of population”, *The Journal of Chemical Physics* **108**(5) (1998).
- [45] I. Degani, A. Zanna, L. SÆlen, and R. Nepstad, “Quantum control with piecewise constant control functions”, *SIAM Journal on Scientific Computing* **31**(5), 3566–29 (2009), copyright - Copyright] © 2009 Society for Industrial and Applied Mathematics; Last updated - 2012-02-12.
- [46] “The n-dimensional coulomb problem and its application to few-particle quantum theory”, Ph.D. thesis.
- [47] M. Abramowitz and I. A. Stegun, *Handbook of mathematical functions with formulas, graphs, and mathematical tables*, volume 55 of *National Bureau of Standards Applied*

Mathematics Series, For sale by the Superintendent of Documents, U.S. Government Printing Office, Washington, D.C., (1964).

- [48] M. Bautista-Moedano and J. L. Lopez-Bonilla, “Matrix elements for the Coulomb interaction”, *Apeiron* **13**, 34–42 (2006).
- [49] B. H. Bransden and C. Joachain, *Physics of Atoms and Molecules*, Pearson Education limited, (2003).